JGR Space Physics

RESEARCH ARTICLE
10.1029/2023JA031817

Distinguishing Electromagnetic Ion Cyclotron (EMIC) Waves From Other Pc1 Signatures in Satellite Recordings by Means of the Swarm Satellite Constellation

Hermann Lühr[1] **and Yun-Liang Zhou**[2]

[1]GFZ German Research Centre for Geosciences, Section 2.3, Geomagnetism, Potsdam, Germany, [2]Department of Space Physics, Electronic Information School, Wuhan University, Wuhan, China

Key Points:

- Resolving for the first time the spatial/temporal ambiguity in satellite wave signals within the Pc1 range by the Swarm constellation
- Small-scale (10s km) quasi-static current features are frequently detected, also medium-scale (100s km) waves with less than 1 Hz are found
- Electromagnetic ion cyclotron waves exhibit long wavelengths (~1,000 km). This has to be verified for their identification

Correspondence to:
H. Lühr,
hluehr@gfz-potsdam.de

Citation:
Lühr, H., & Zhou, Y.-L. (2023). Distinguishing electromagnetic ion cyclotron (EMIC) waves from other Pc1 signatures in satellite recordings by means of the Swarm satellite constellation. *Journal of Geophysical Research: Space Physics*, *128*, e2023JA031817. https://doi.org/10.1029/2023JA031817

Received 25 JUN 2023
Accepted 4 NOV 2023

Abstract In this study we make use of the closely spaced Swarm A and C spacecraft to determine the main wave parameters of micro-pulsation in the Pc1 range. Generally, the interpretation of wave events in satellite recordings suffers from the spatial/temporal ambiguity of such data. To resolve that problem, we use for the first time in the 0.2–5 Hz apparent frequency range high-resolution magnetic field data from the Swarm A/C spacecraft pair. Particularly suitable for this analysis is the period of Counter Rotating Orbit Phase in 2021. During that period the along-track distance between the spacecraft was varied from 2 to 40 s. Surprisingly many of the wavy signals at middle latitudes were identified as small-scale (order of 10s km) quasi-static field-aligned current (FAC) structures. Some of the events turned out to be medium-scale (100–200 km) waves oscillating at 1 Hz or less. A number of published electromagnetic ion cyclotron (EMIC) waves were checked on their consistency. One characteristic is their long wavelength (~1,000 km). About half of the cases passed the check, the other did not satisfy the spatial homogeneity. The small-scale FAC structures we believe to be driven by atmospheric gravity waves. While the medium-scale waves we prefer to relate to the effects of the ionospheric Alfvén resonator.

1. Introduction

Geomagnetic pulsations in the frequency range from 0.2 to 5 Hz are termed Pc1. Their properties have been studied by ground-based observations for many decades. They are frequently detected in subauroral regions. Various studies showed their appearance in close relation with proton auroras (e.g., Sakaguchi et al., 2008; Yahnin et al., 2009). Rather well-excepted is the appearance of Pc1 in connection with a rapid dropout of radiation belt relativistic electrons (e.g., Miyoshi et al., 2008; Yuan et al., 2018). Furthermore, it had been predicted that Pc1 pulsations could be caused by standing Alfvén waves trapped in the ionospheric Alfvén resonator (IAR). These oscillations can last quite long when the driving wave matches the IAR normal frequency (Lysak et al., 2013).

Ground-based observations of Pc1 are available since magnetometers provided sufficient amplitude and time resolution (see Mursula et al., 1994 for a historical overview and Kangas et al., 1998 for a review). Many of these waves have been attributed to the action of the IAR. Between the E-region and the lower magnetosphere their exists an Alfvén velocity peak. Waves fitting the resonance frequency within this cavity (commonly overlapping with the Pc1 range) can oscillate for quite a long time. For more details see Belyaev et al. (1990).

In this study we focus on Pc1 observations by low-Earth orbit (LEO) satellites. These spacecraft travel fast (~7.5 km/s) through the ionosphere. Therefore, both spatial structures and wave events can contribute to magnetic variations in the Pc1 frequency range. Earlier studies based on for example, Magsat (Iyemori & Hayashi, 1989) or Space Technology 5 (ST-5) (Engebretson et al., 2008) did not separate these two effects efficiently. Park et al. (2013) were the first to provide a comprehensive overview of clear Pc1 signatures in the 10-year data set of the CHAMP mission. They seriously tried to exclude contributions from spatial structures, such as small-scale FACs in the auroral region or those connected with ionospheric irregularities at low latitudes (e.g., plasma bubbles). From their long and homogeneous data set, the authors have deduced a number of typical wave characteristics. Events are detected preferably at subauroral latitudes and near longitudes connected to the region of the South Atlantic Anomaly (SAA). More events occur on the night than on the dayside. Local summer is a preferred season in both hemispheres.

The EMIC waves are considered to be an important source for the Pc1. These waves are generated in the magnetosphere at near equatorial latitudes. They have attracted quite some interest since they play an important role in the scattering of energetic particles out of the radiation belt. On their way, propagating along field lines, from the magnetosphere to the ionosphere the waves may experience a number of property changes, concerning frequency content and polarity (e.g., Denton et al., 1996; Min et al., 2012). Within the ionosphere the resulting Pc1 can be ducted across the magnetic field, allowing observations at locations not conjugate to the EMIC source region (e.g., Lysak & Yoshikawa, 2006). Kim et al. (2010) were probably the first to present observations of an EMIC event both from ground and LEO satellite. By good fortune a CHAMP overpass occurred at the time and location of Pc1 ground recordings in the Antarctic region. Both instruments measured frequencies near 0.5 Hz and similar amplitude structures. Common observability in the ionosphere and on the ground requires long wavelengths, of the order of 1,000 km. During subsequent years many more studies appeared (mainly based on Swarm B-field data) that interpreted the LEO Pc1 recordings as ionospheric signatures of EMIC waves (e.g., Kim et al., 2020, 2021; Wang, He, & Lühr 2022; Wang, Sun, et al., 2022; Wang et al., 2019, 2021).

All these statistical studies have disclosed important properties of EMIC wave. However, there exists a caveat. Single spacecraft observations cannot distinguish between spatial and temporal structures from their observations, and they provide no information about the wavelength. It may well be assumed that a part of the detected events does not represent EMIC waves. Those will bias the statistic.

In this study we make use of the Swarm constellation comprising three identical spacecraft. When properly spaced they can uniquely determine the main wave features like frequency, wavelength, and propagation direction. Very good conditions for such investigations occurred during the Swarm counter-rotation period in 2021, when all three spacecraft orbited practically in the same plane but partly (e.g., Swarm B) in opposite direction. Part of this formation campaign was dedicated to variations of the along-track separation between Swarm A and C from 2 to 40 s, which corresponds to distances from 15 to 300 km. But also, the standard configuration, with Swarm A and C separated by 1.4° in longitude and following each other at a distance of 30–75 km, is suitable in many cases to derive the main Pc1 wave properties.

In the section to follow the instrumentation and data set will be introduced, followed by an outline of the applied dual-satellite wave analysis. Subsequently we present in Section 3 three kinds of observed wave types. For those recorded oscillations their frequencies and wavelengths are determined. In Section 4 the main properties of different waves are discussed and compared with earlier reported findings. Finally, we are summarizing the main results.

2. Instrumentation and Data Set

ESA's Swarm mission was launched on 22 November 2013. It consists of three identical satellites in near-polar orbits at different altitudes. Maneuvers for the first constellation mission phase were completed on 17 April 2014. For that Swarm A and C flew side-by-side (separated by 1.4° in longitude) at an initial altitude of 460 km, while Swarm B orbited 50 km higher. During the subsequent years the height slowly decreased. Due to their orbital precession, Swarm A and C need about 133 days to cover 24-hr local time (LT), while for Swarm B it takes about 141 days.

During the second mission phase, the so-called counter-rotating orbit phase, starting in October 2019, the longitudinal separation between Swarm A and C was slowly reduced. After almost 8 years in orbit a quasi-coplanar configuration was achieved between the Swarm A/C pair and Swarm B. Around 4 October 2021 the orbital planes of Swarm A/C and Swarm B crossed near the equator. Coinciding with that event the longitude separation between Swarm A and C went through zero, having them orbit coplanar. The along-track separation between Swarm A and C is generally kept in the range 4–10 s. Starting from 1 July 2021 this was also reduced. As shown in Figure 1, for about 2 months it was maintained at 4 s. After that a 2-week period of only 2 s separation between the spacecraft followed, coinciding with the quasi-proper counter-rotation. From 6 October 2021 onward, the along-track separation was steadily increased until reaching 40 s in the first half of December. After that the separation was rapidly reduced, attaining the normal along-track spacing again by middle of January 2022. The periods of varying spacecraft separations are very well suited for determining the spatial scales of wave signatures.

Each of the three satellites is equipped with a set of six instruments (Friis-Christensen et al., 2008). In this study, we use the data from the Vector Field Magnetometer (VFM), a fluxgate magnetometer taking 3-component

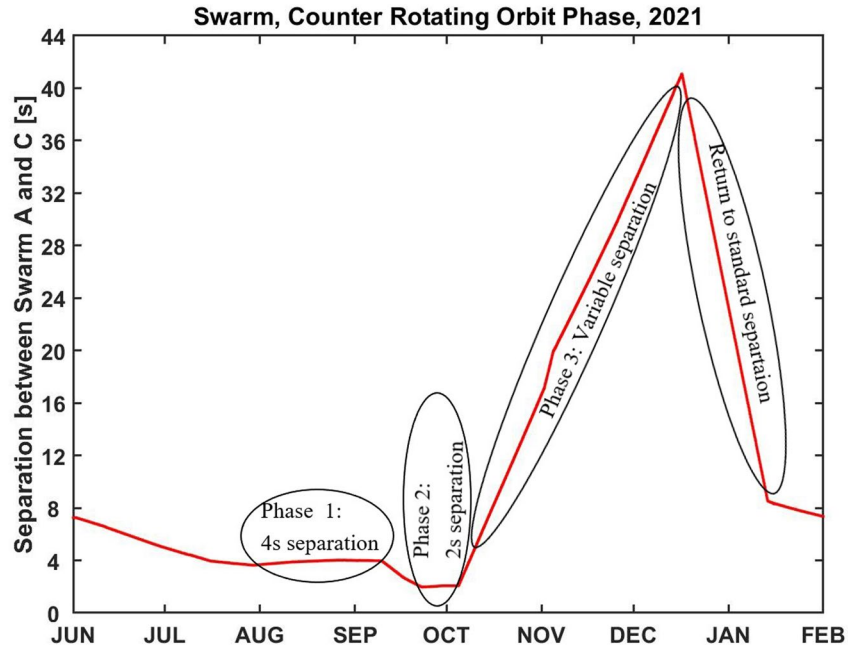

Figure 1. Variation of the controlled along-track separation changes between Swarm A and C during the Counter Rotation Orbit Phase. At times of standard operation the inter-spacecraft separation is kept within the range of 4–10 s, as during intervals at the beginning and end of the displayed period.

readings at a rate of 50 Hz. This instrument is routinely calibrated against the Absolute Scalar Magnetometer (ASM), in order to maintain high precision over the mission duration.

The data product we utilized is Swarm Level 1b MAGx_HR, which includes the vector magnetic field recordings at a time-resolution of 50 Hz. To remove the large-scale background field, we also employed the magnetic recordings at 1 Hz resolution, provided as part of Swarm Level 1b MAGx_LR. For both data products we used the latest version (0602). All these data can be downloaded from the European Space Agency website (https://earth.esa.int/web/guest/swarm/data-access).

For our analysis of the wave characteristics, we first check the eastward, *By*, component. It has been shown before (e.g., Kim et al., 2018; Park et al., 2013) that most of the signal in the Pc1 frequency range appears in this component. When a Pc1 event was identified, we determine the polarization direction of the wave, which is found to be close to linear and transverse to the ambient field direction. For the interpretation we make use of the full wave signal, the maximum variation component.

For isolating the Pc1 signal in the magnetic field recordings, the 50 Hz data have been band-pass filtered. For the upper end the cut-off frequency (−3 dB) of the low-pass filter is set to 5 Hz. This reduces the digitization noise. For suppressing the mean-field variations and lower-frequency pulsations, the 1 Hz data are low-pass filtered with a cut-off at 0.1 Hz. Then the slowly varying signals are subtracted from the 50 Hz field data.

The Pc1 events, we are interested in, are commonly well isolated in frequency space. This makes it possible to distinguish them from encounters of auroral FACs and the traverses through equatorial plasma depletions. In both these cases broadband signals are observed, covering the whole displayed frequency range.

2.1. Dual-Satellite Wave Analysis

The closely spaced satellite pair, Swarm A and C, allows to resolve the temporal spatial ambiguity of harmonic variations in spacecraft recordings. When observing waves with two satellites following each other, the signal at the two spacecraft can be expressed as follows

$$\mathrm{Sw}A = A\cos(\omega t + kx_A + \varphi) \quad (1)$$

$$\mathrm{Sw}C = A\ \cos(\omega t + k(x_C - x_{\Delta AC}) + \varphi) \tag{2}$$

where A is the amplitude, ω is the cycle frequency, t is time, k is the wavenumber component in flight direction, x_A and x_C are along-track positions, $x_{\Delta AC}$ is along-track spacecraft separation and φ is a phase.

In the case of a satellite, t and x do not vary independently. Therefore, x can be substituted by x (km) = v t (s), where v = 7.5 km/s represents the spacecraft velocity and k has the unit rad/km. Furthermore, the start time of t can be chosen that φ disappears.

$$\mathrm{Sw}A = A\ \cos[(\omega + v\,k)t] \tag{3}$$

$$\mathrm{Sw}C = A\ \cos[(\omega + v\,k)t + v\,k\Delta t] \tag{4}$$

where Δt is the along-track time separation between Swarm A and C. From these equations we see that the apparent frequency in the recordings is determined by the sum of ω plus $v\,k$. Depending on their relative values, one of the two quantities may dominate the sum. In the following we will consider three different types of wave signals: quasi-stationary structures, waves with medium wavelength and large-scale waves.

Examples of the first case show practically no temporal changes. Thus, we can neglect ω in the sum and get for the two satellites

$$\mathrm{Sw}A = A\ \cos(v\,kt) \tag{5}$$

$$\mathrm{Sw}C = A\ \cos[v\,k(t + \Delta t)] \tag{6}$$

The stationarity can be checked by a cross-correlation analysis. In the ideal case the readings of Swarm C can be made match those of Swarm A at a time shift that fits the distance between the spacecraft. The transverse scale-length in flight direction of the current structure can be determined from the oscillation period times the satellite velocity.

In the case of medium-scale waves, when ω and $v\,k$ are of comparable size, the full equations, Equations 3 and 4, have to be considered for deriving the wave parameters. Here the formula for Swarm C can be decomposed by the addition theorem.

$$A\ \cos[(\omega + v\,k)t]\cos(v\,k\Delta t) - A\ \sin[(\omega + v\,k)t]\sin(v\,k\Delta t) \tag{7}$$

For our evaluation we also consider the difference, SwC − SwA.

$$\mathrm{Sw}C - \mathrm{Sw}A = A\ \cos[(\omega + v\,k)t]\cos(v\,k\Delta t) - A\ \sin[(\omega + v\,k)t]\sin(v\,k\Delta t) - A\ \cos[(\omega + v\,k)t] \tag{8}$$

In case ($vk\Delta t$) is small (e.g., <π/4), practically only the sine-part matters and we can approximate the signal difference by

$$\mathrm{Sw}C - \mathrm{Sw}A = A\ \sin[(\omega + v\,k)t]\sin(v\,k\Delta t) \tag{9}$$

By fitting harmonic functions to the observed signal of Swarm A and to the differences between the spacecraft recordings we can solve for the wave parameters: amplitude, frequency and wavelength.

In the third case we assume really large wavelengths and consequently small wave numbers, k. For such cases the wave equations can be simplified.

$$\mathrm{Sw}A = A\ \cos(\omega t) \tag{10}$$

$$\mathrm{Sw}C = A\ \cos[\omega t + v\,k\Delta t] \tag{11}$$

These events show practically identical wave signatures in the Swarm A and C recordings. From the still existing small time lag (T-lag), compared to the wave period, P, the phase shift, φ, at Swarm C can be determined,

$$\varphi = 2\pi\frac{T - \mathrm{lag}}{P} = v\,k\Delta t \tag{12}$$

and subsequently solved for the along track wavenumber

Table 1
Listing of Pc1 Wave Polarization Properties

Fig	Sw	Time interval, UT	Polariz. angle deg	Angle (v,n) deg
2	A	00:45:20–00:47:10	−15.64	67.31
		00:47:10–00:48:10	−23.9	57.72
3	A	16:26:20–16:26:50	−16.12	52.47
		16:26:50–16:28:50	−3.43	52.43
		16:36:00–16:37:35	−11.75	54.95
		16:37:35–16:38:00	−17.38	50.02
4	A	21:51:00–21:55:00	−6.5	57.72
5	A	09:31:00–09:33:20	−16.65	26.45
		09:33:20–09:33:50	−68.36	67.20
6	A	19:21:15–19:21:40	−29.73	63.04
		19:21:45–19:22:15	−27.7	61.12
		19:22:15–19:23:30	−0.57	38.84
		19:23:45–19:24:30	−3.15	40.09
8	A	20:49:40–20:54:30	5.26	33.06
10	A	19:48:05–19:48:20	−7.05	39.5
11	A	20:53:30–20:57:20	0	40.08
12	A	15:43:20–15:46:10	−19.60	51.22
		16:03:15–16:06:05	−19.60	27.75
13	A	16:39:55–16:40:45	−9.26	27.27
		17:00:25–17:01:45	17.48	22.53
14	A	17:18:00–17:18:40	−27.27	23.29
	A	17:18:40–17:18:55	−53.97	45.87
	B	17:17:52–17:18:32	−27.27	23.28
	B	17:18:32–17:18:47	−53.97	45.84
	C	17:18:14–17:18:54	−27.27	23.32
	C	17:18:54–17:19:09	−53.97	45.91
15	A	15:10:15–15:10:35	25.13	30.02
	C	15:10:12–15:10:32	25.13	29.76

Note. For the events presented in the various figures (partly several separate intervals) the polarization angle with respect to magnetic east and the angle between the spacecraft velocity and the wave normal (v,n) are listed.

$$k = 2\pi \frac{T - \text{lag}}{P} \frac{1}{v\Delta t} \tag{13}$$

Wave amplitude and frequency can be derived directly from the fitting to the Swarm A recordings.

3. Observations

For the evaluation of the Pc1 wave properties we routinely produced *By* component wave spectrograms from the Swarm A magnetic field data. We started with the time period when the separation between Swarm A and C was smallest. Here the reproducibility of the magnetic field structure, observed by the two spacecraft, can be tested best. From Figure 1 it can be seen that the 2-s separation lasted from 20 September to 6 October 2021. Within this 2-week period several events with waves in the 0.2–5 Hz frequency range have been observed. Subsequently, also other time periods were considered to obtain a larger variety of wave events.

For the characterization of the wave events, we show in the following only one magnetic field component. This is aligned with the direct of maximum variation and is termed *Bw*. Such a confinement is justified because the presented waves are close to linearly polarized. In Table 1 the angles are listed by which *Bw* differs from the magnetic eastward direction. For some of the considered events there are several angles listed. This indicates that the direction of maximum variations differs significantly for some of the wave packet within the displayed time series.

Based on a first inspection of the signal differences between the spacecraft we have sorted the events into three classes. If practically no temporal change between the passages of the spacecraft Swarm A and C are detectable, the observed structure is classified as quasi-stationary. Conversely, if both Swarm A and C observe simultaneously the same wave signal although they are separated by more than 100 km, such an event is classified as large-scale wave. The remaining cases, where both spatial and temporal variations have to be considered from the simultaneous Swarm A and C observations are termed medium-scale waves. In the following three subsections we will first present examples of quasi-static events. These represent obviously small-scale FAC structures. Next, we look at medium-scale wave events, and finally, examples of large-scale waves are studied.

3.1. Quasi-Static Current Structures

A typical example of a quasi-stationary wave structure is shown in Figure 2. The top frame shows the signal spectrum of a pass early 28 September 2021 within the 21hr magnetic local time (MLT) sector. At high latitudes very intense broad-band signal is apparent, which is caused by auroral FACs. These features are of no concern here. At low latitudes also several broad-band wave bursts appear. They are probably associated with equatorial plasma irregularities (plasma bubbles). We focus on the strongest signal at low frequencies (red framed). Below the spectrum high-resolution magnetic field recordings from the two spacecraft are plotted. The lower panel presents the simultaneously recorded data by the two spacecraft. The labels below give measurement time and the corresponding magnetic latitudes, separately for Swarm A and C. In the upper panel the signal is repeated, but the Swarm C data is shifted by 2.1 s. This time difference practically reflects the actual along-track separation of the satellites. The $\Delta t = 1.95$ s, also listed in the frame heading, is the determined time difference between the equator crossings. When taking the optimal time shift into account, we achieve an almost perfect match with a correlation coefficient of CC = 0.98. A visual inspection also confirms that the differences of the curves amount only to a few pT, also confirming the high

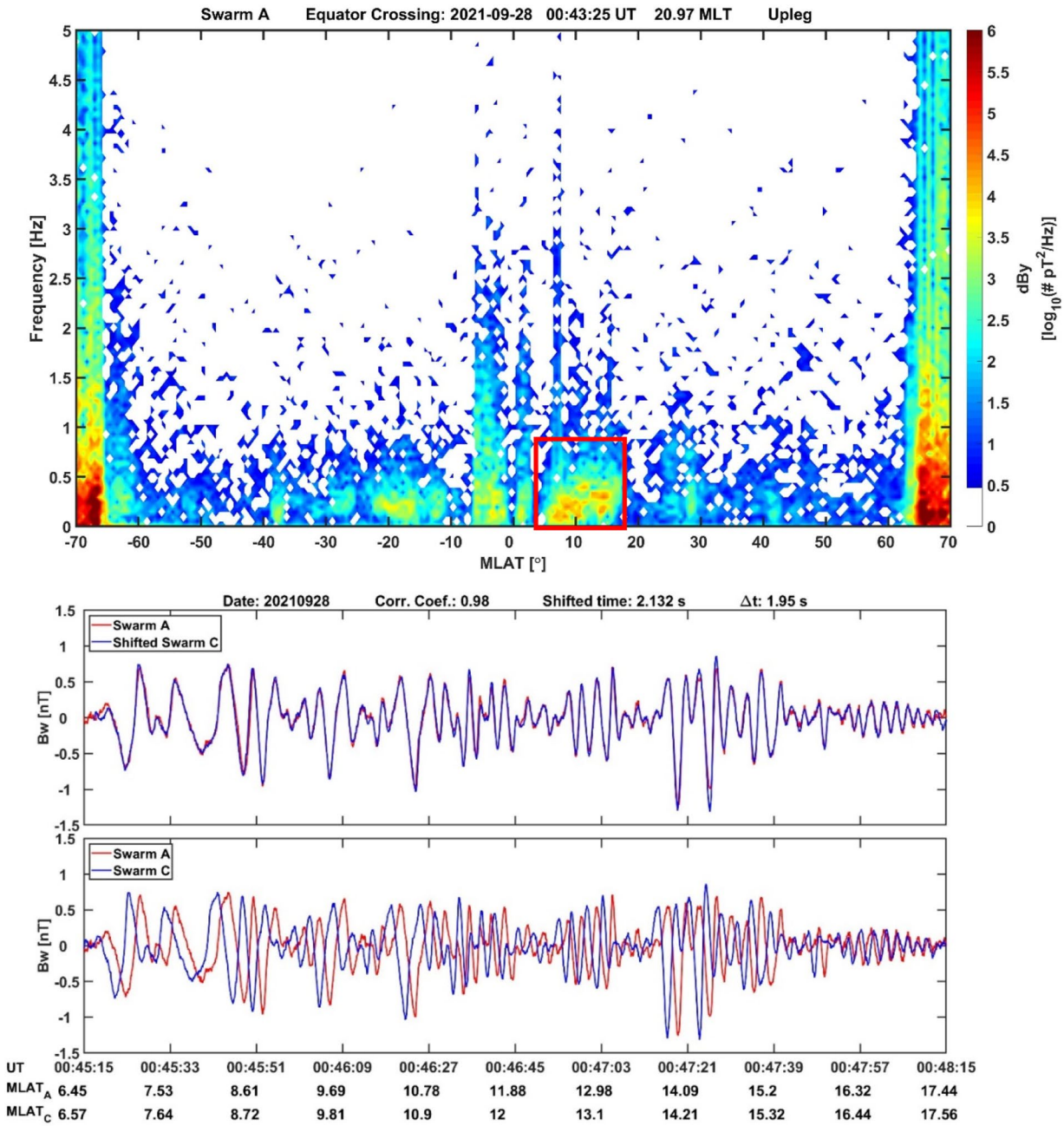

Figure 2. Example of wavy magnetic field signal recorded by Swarm A and C. The spectrogram in the top frame shows the activity in the Pc1 range during the satellite pass quoted in the heading. Time series of the signal marked by the red square in the spectrum are shown below. The bottom panel displays the simultaneous recordings of Swarm A and C. The labels below list the measurement time (UT) and the corresponding magnetic latitudes of the two spacecraft. When providing an optimal time shift to the Swarm C data a high degree of correlation is achieved between the recordings. This time shift is almost identical to the time difference, Δt, between the equator crossings of the two spacecraft.

quality of the two independent magnetic field measurements. For this event we can state, the two Swarms flew through a spatial magnetic field structure that did not change within 2 s. The apparent mean frequency of about 0.33 Hz converts to an along-track wavelength of 23 km, considering the on-orbit velocity of 7.5 km/s. From the angle between the velocity and the wave normal (v,n), right column of Table 1, top two lines, we can estimate the perpendicular wavelength, $\lambda_{perp} = \lambda\cos(v,n)$. This results in actual wavelengths of less than 10 km.

In several cases, Pc1 wave packets show up at conjugate latitudes. One such example is shown in Figure 3. Here the Swarm satellites detect harmonic variations around 20° MLat in the two hemispheres (see red frames in

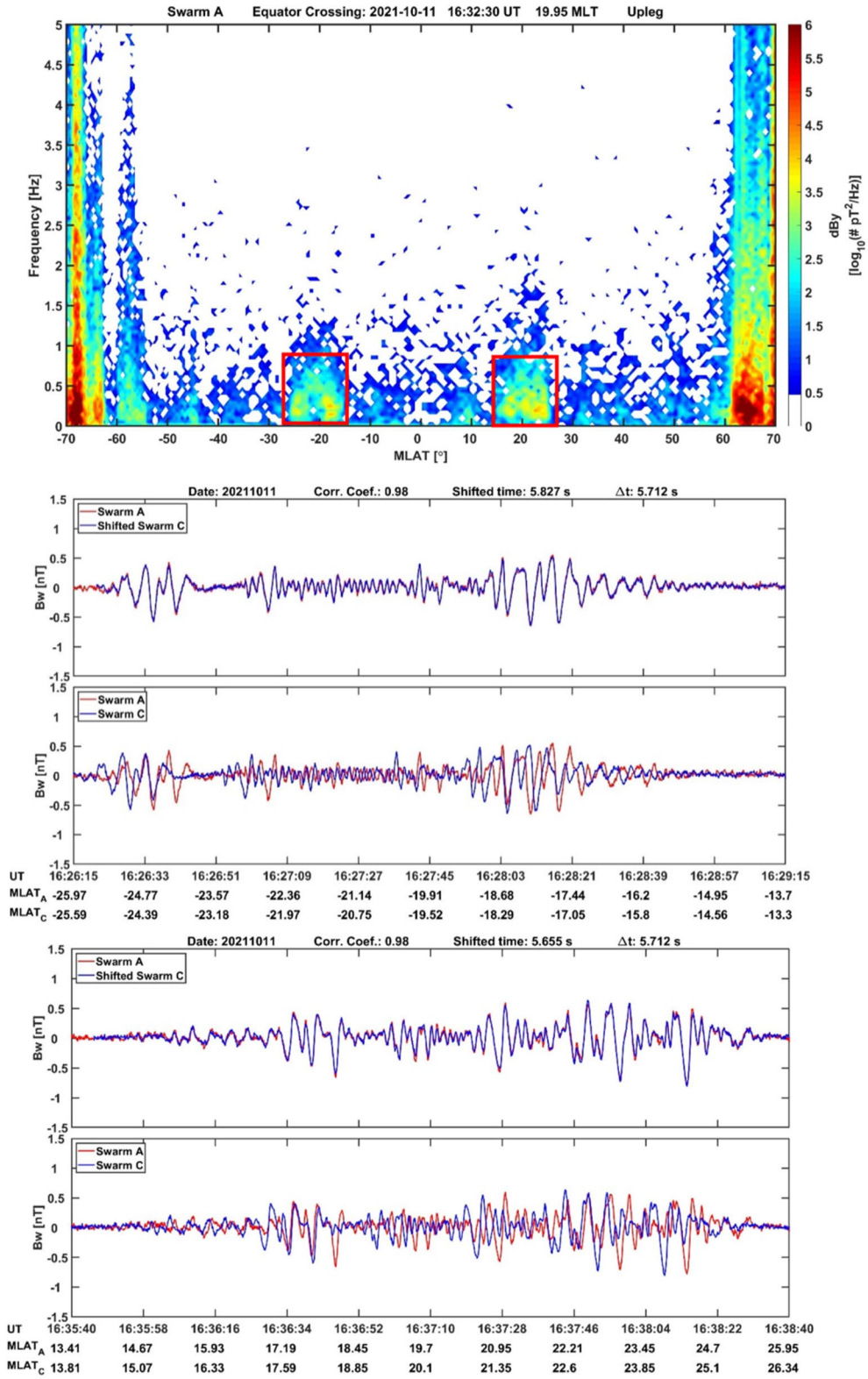

Figure 3. The same as Figure 2, but for examples from 11 October 2021.

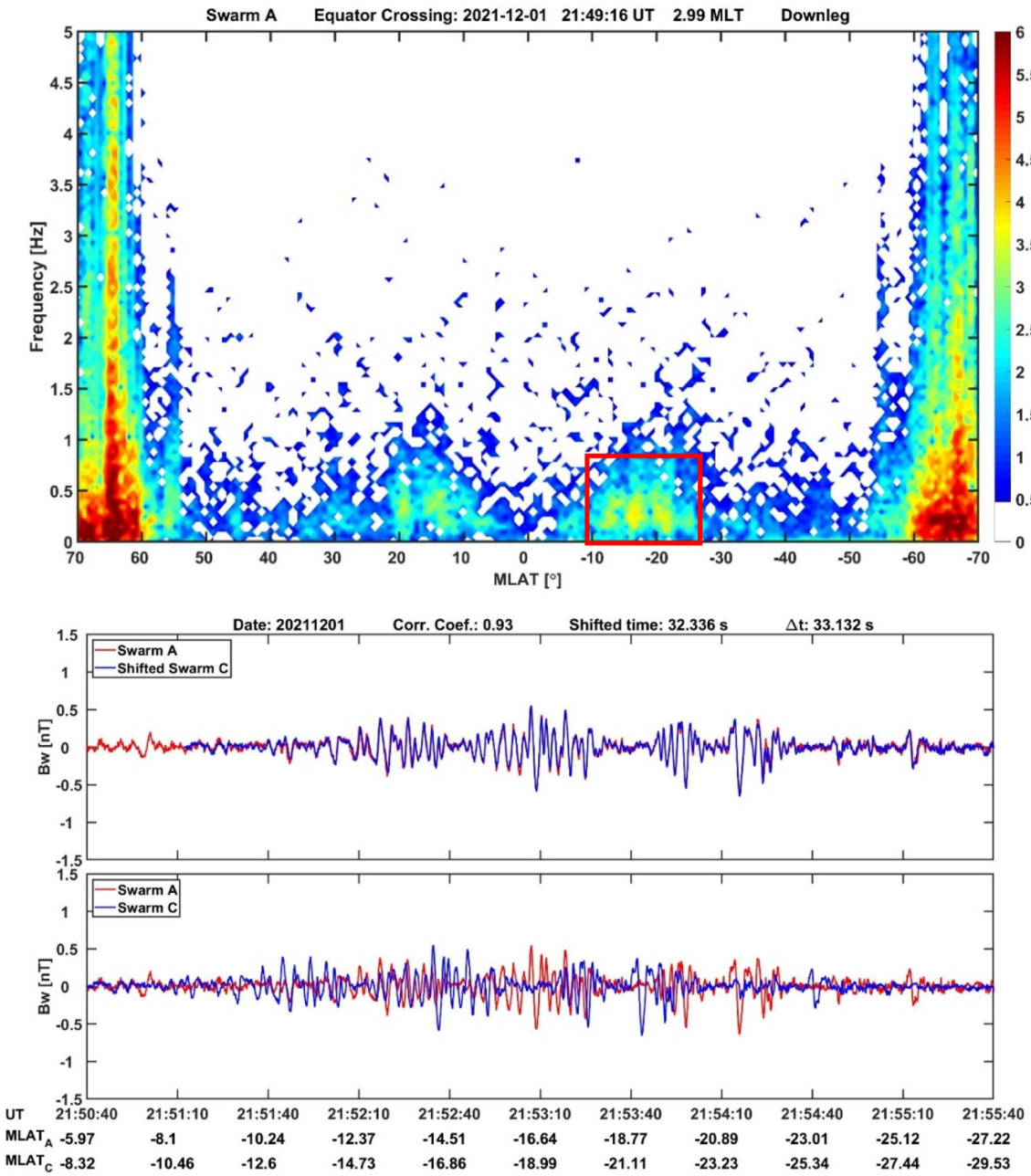

Figure 4. The same as Figure 2, but for an example from 1 December 2021.

spectrum). The magnetic field recordings can again be made match (CC = 0.98) when delaying the Swarm C recordings. A mean time shift of about 5.7 s is found in both hemispheres and agrees well with the along-track time difference of 5.7 s. This shows, Swarm has crossed spatial structures that did not change within 6 s. Encountered wavelengths range between 10 and 30 km when considering the transverse scales.

We tested some low-latitude structures with even longer spacecraft separations. Figure 4 presents a case similar to that as shown in Figure 3. The difference is that we have inter-spacecraft time differences of $\Delta t = 33.1$ s at the equator, but even at that separation excellent agreements with CC = 0.93 is achieved when properly shifted. This demonstrates, these spatial structures with wavelengths of some 10s of km are stable over a significant amount of time.

Many of the Pc1 studies focus on the detection of EMIC wave. These appear preferably at subauroral latitudes, conjugate to their source region in the magnetosphere (e.g., Wang et al., 2019). Figure 5 presents a wave event in this region, around −56° MLat. Both the latitude and spectral peak at 1 Hz fit well the characteristics of EMIC wave.

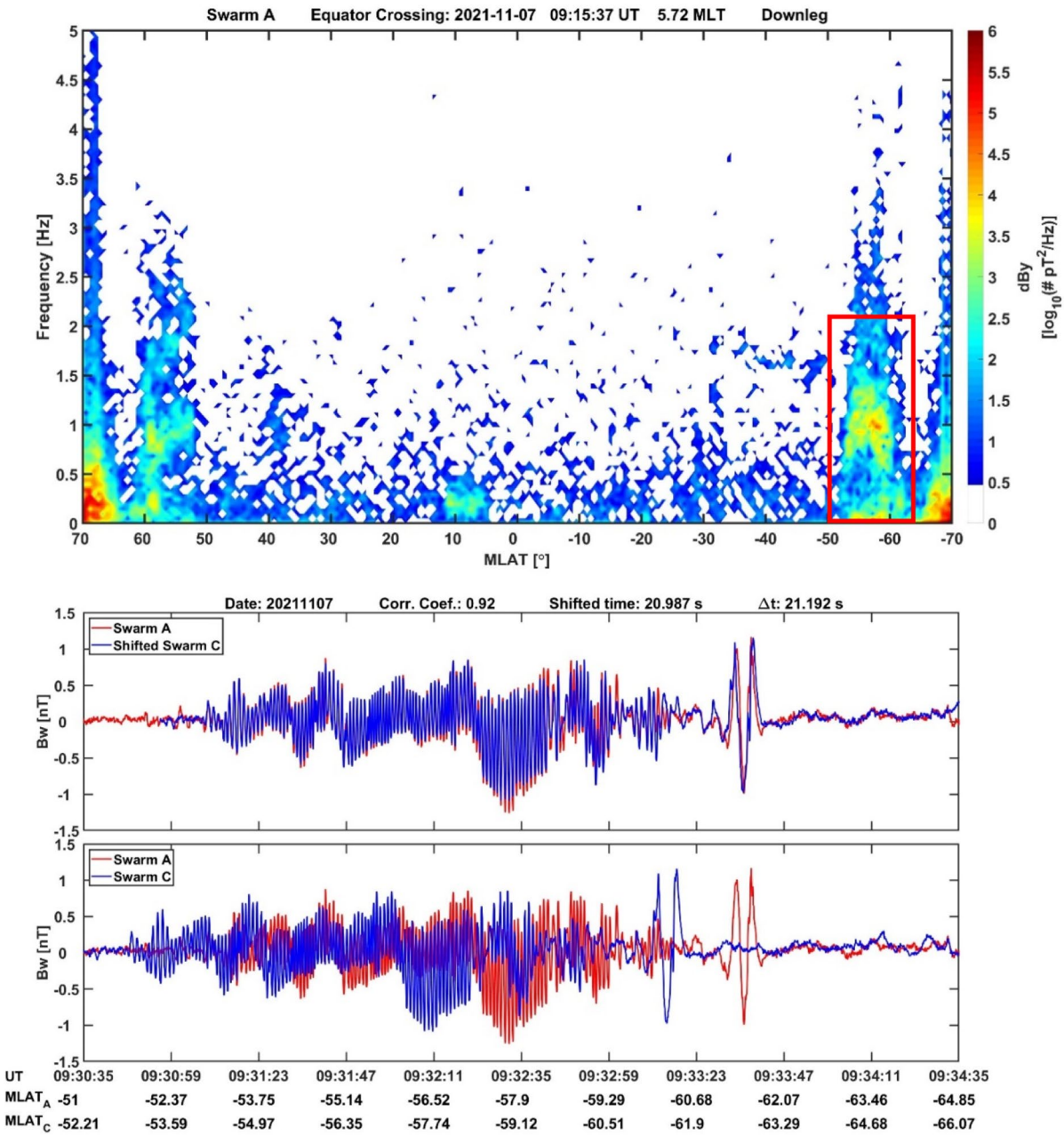

Figure 5. The same as Figure 2, but for an example from 7 November 2021.

When looking at the original recordings of Swarm A and C (bottom panel), quite different variations are observed. Things change significantly when Swarm C data are delayed by 21 s. Then the signals match very well. It is impressive how all the apparent 1 Hz oscillations line up so nicely, as reflected by the correlation coefficient of 0.92. These 6-km wavelength structures have only changed a little in amplitude between the times of visits ($\Delta t = 21.2$ s) by the two Swarm spacecraft. Here the cross-correlation has been confined to the interval of the 1-Hz signal. This small-scale case adds to the variety of quasi-static spatial structures that must not be confused with EMIC wave events.

3.2. Medium-Scale Pc1 Waves

There are also wave-like events observed where the differences between the recordings of Swarm A and C are smaller but the signals cannot be made matched by a time shift. An example for that is shown in Figure 6. The dynamic spectrum in the top frame shows in the southern subauroral region a wave feature with rising frequency

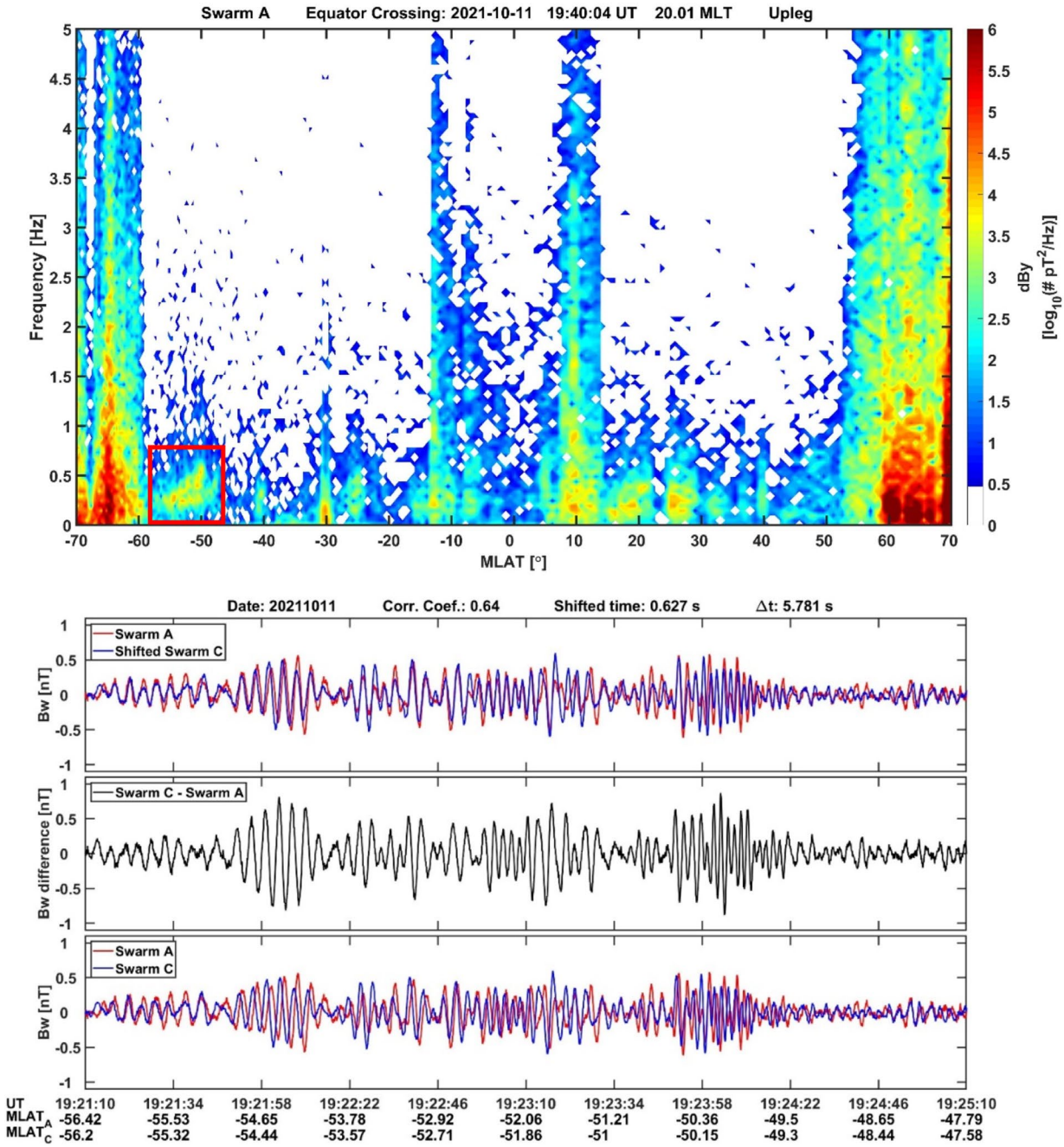

Figure 6. Example of an event with increasing apparent frequency. Here the simultaneous recordings from Swarm A and C (bottom panel) differ only slightly. However, no good overall correlation can be achieved by a time shift (top panel). The middle panel shows the difference between the simultaneously recorded Swarm A and C signals. This is used for the estimation of wave parameters.

(red frame). Time series plots from both satellites are shown in the bottom panel. Confined wave packets appear, for which the apparent frequency increases from package to package toward lower latitudes. A cross-correlation applied to the whole interval is not so successful to match the two time series, as in the cases shown before. It achieves only a CC = 0.64 at a shift of 0.6 s. This is significantly shorter than the actual time difference between the satellites of 5.8 s. It is also evident from the top panel in the lower frame, the time shift cannot satisfy a signal match for all wave packages equally well. Here we obviously observe a case where temporal and spatial variations have to be considered for the interpretation. The independent observations from the two Swarm satellites can help to resolve this ambiguity.

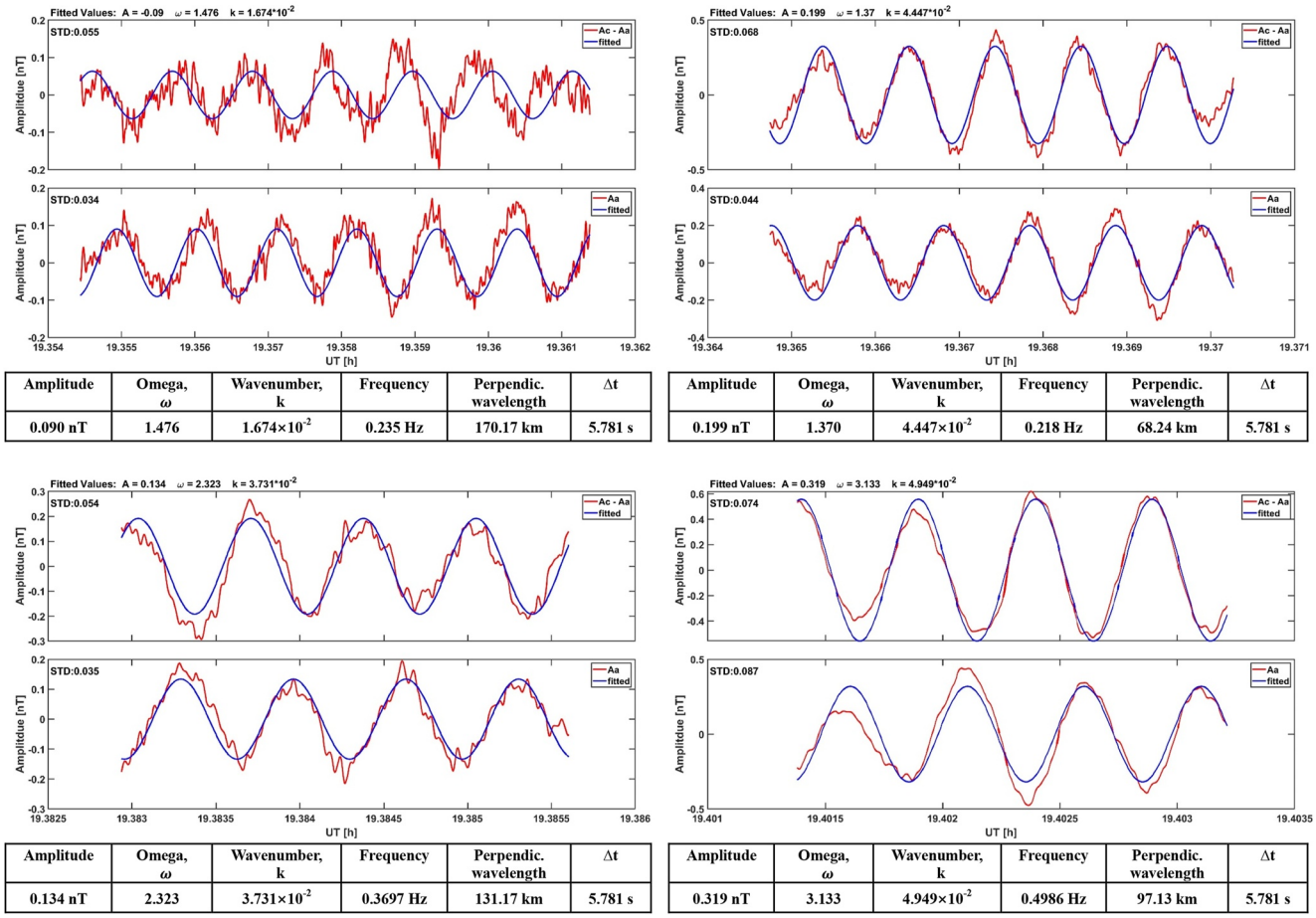

Amplitude	Omega, ω	Wavenumber, k	Frequency	Perpendic. wavelength	Δt
0.090 nT	1.476	1.674×10^{-2}	0.235 Hz	170.17 km	5.781 s

Amplitude	Omega, ω	Wavenumber, k	Frequency	Perpendic. wavelength	Δt
0.199 nT	1.370	4.447×10^{-2}	0.218 Hz	68.24 km	5.781 s

Amplitude	Omega, ω	Wavenumber, k	Frequency	Perpendic. wavelength	Δt
0.134 nT	2.323	3.731×10^{-2}	0.3697 Hz	131.17 km	5.781 s

Amplitude	Omega, ω	Wavenumber, k	Frequency	Perpendic. wavelength	Δt
0.319 nT	3.133	4.949×10^{-2}	0.4986 Hz	97.13 km	5.781 s

Figure 7. Fitting of the wave functions, Equations 8 and 3 to the differences, Swarm C minus Swarm A, and the recording of Swarm A, respectively. Shown are cases for the wave packets around 19:21:30, 19:22, 19:23, 19:24 UT. The derived main wave parameters are listed below the frames.

We are observing one wave with two satellites, following each other. As part of the interpretation of the event shown in Figure 6, we tried to estimate the wave parameters by first fitting the function for Swarm A (Equation 3) to the observations, in order to determine the amplitude, A and the sum, $(\omega + v\,k)$. Furthermore, we consider the difference between the two simultaneously observed oscillation, which is shown in the middle panel of Figure 6. The above derived wave quantities are inserted into Equation 8, and then that function is fitted to the observed difference curve. In this way the last quantity, $v\,k$, is determined. With that we can estimate all the wave parameters: amplitude, frequency and wavelength.

From the illustration in Figure 6 it is already clear that the character of the wave changes from packet to packet. Therefore, our fitting approach has been applied separately to four packets. Subframes in Figure 7 show for each case in the top panel the achieved fitting to the wave-difference curve and in the bottom panel the fitting to Swarm A recordings over the time of the individual wave packet. For all the cases satisfying matches have been achieved between observation and wave function. From the derived wave parameters, listed below the subframes, we see that the frequency is somewhat increasing from 0.2 to 0.5 Hz toward lower latitude. Whereas, the perpendicular wavelength of the first packet amounts to (170 km), somewhat larger than that for the other three packets of above 100 km.

Another such kind of wave event with rising frequency toward lower latitude was observed on 30 September 2021 also at southern subauroral latitudes. Figure 8 shows the spectrogram and below the time series of the interesting part. Here again a good match between the recordings of Swarm A and C is not possible by shifting one of the series. The obtained time shift for best correlation is much smaller than the actual time difference of 2.07 s between the two spacecraft. We applied the same processing approach as before for evaluating the wave

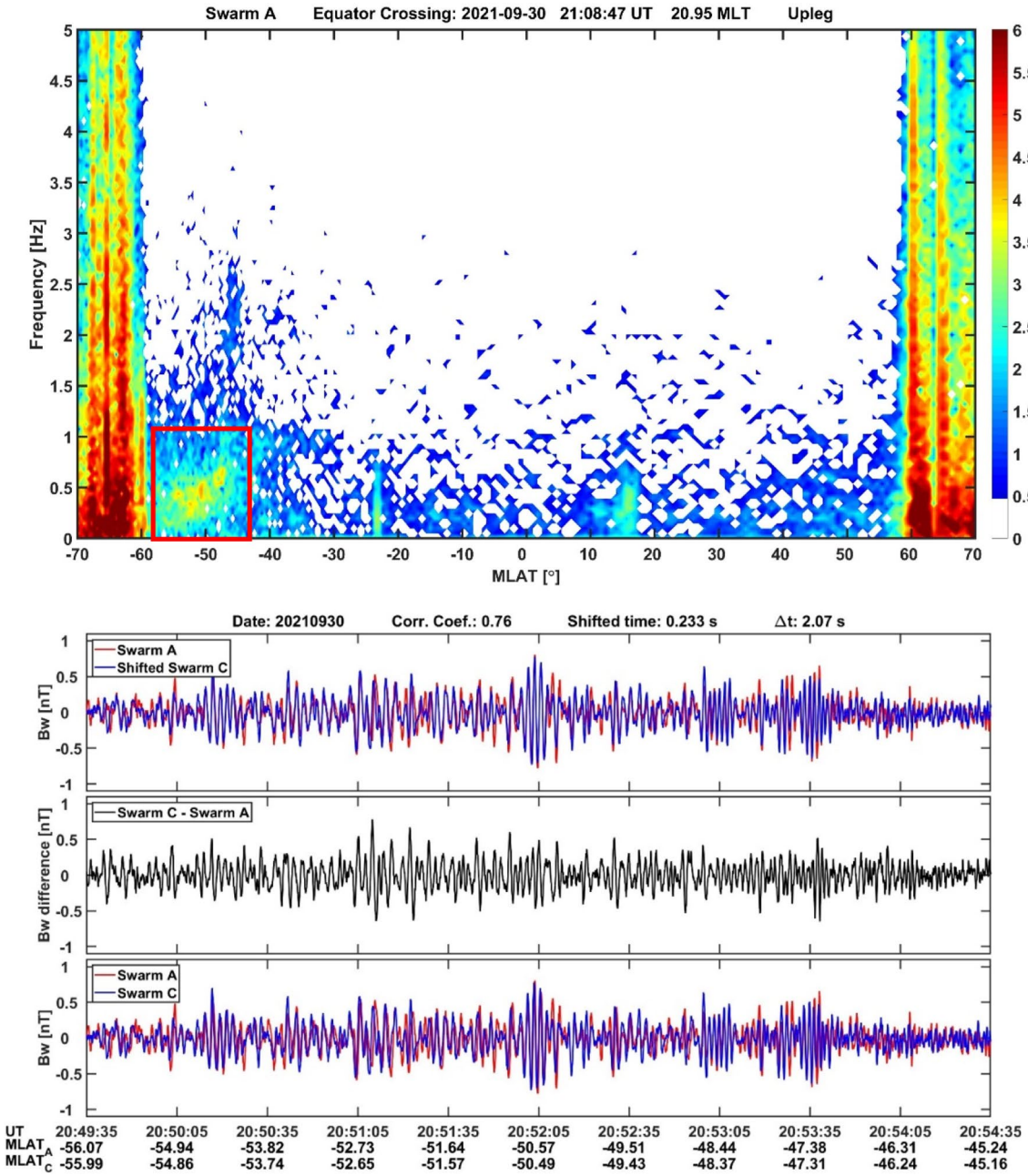

Figure 8. The same format as Figure 6, but for an event on 30 September 2021.

parameters. The subframes in Figure 9 show in the same format as Figure 7 the achieved fittings of wave functions to the four observed wave packages. The results are well comparable with the parameters we obtain for the previous event. Also, the wavelengths vary around 100 km, and the frequency increases gradually from about 0.4 to 0.6 Hz. The similarity between the presented cases suggests that both are of the same wave type. A possible generation mechanism for them is the ionospheric Alfvén resonator.

3.3. Large-Scale Pc1 Waves

In a number of publications authors relate Pc1 oscillations, observed by LEO satellites, to EMIC waves (e.g., Kim et al., 2020, 2021; Wang, He, & Lühr 2022; Wang, Sun, et al., 2022; Wang et al., 2019, 2021). All of their results are based on single-satellite recordings, which do not allow to resolve the spatial/temporal ambiguity. One

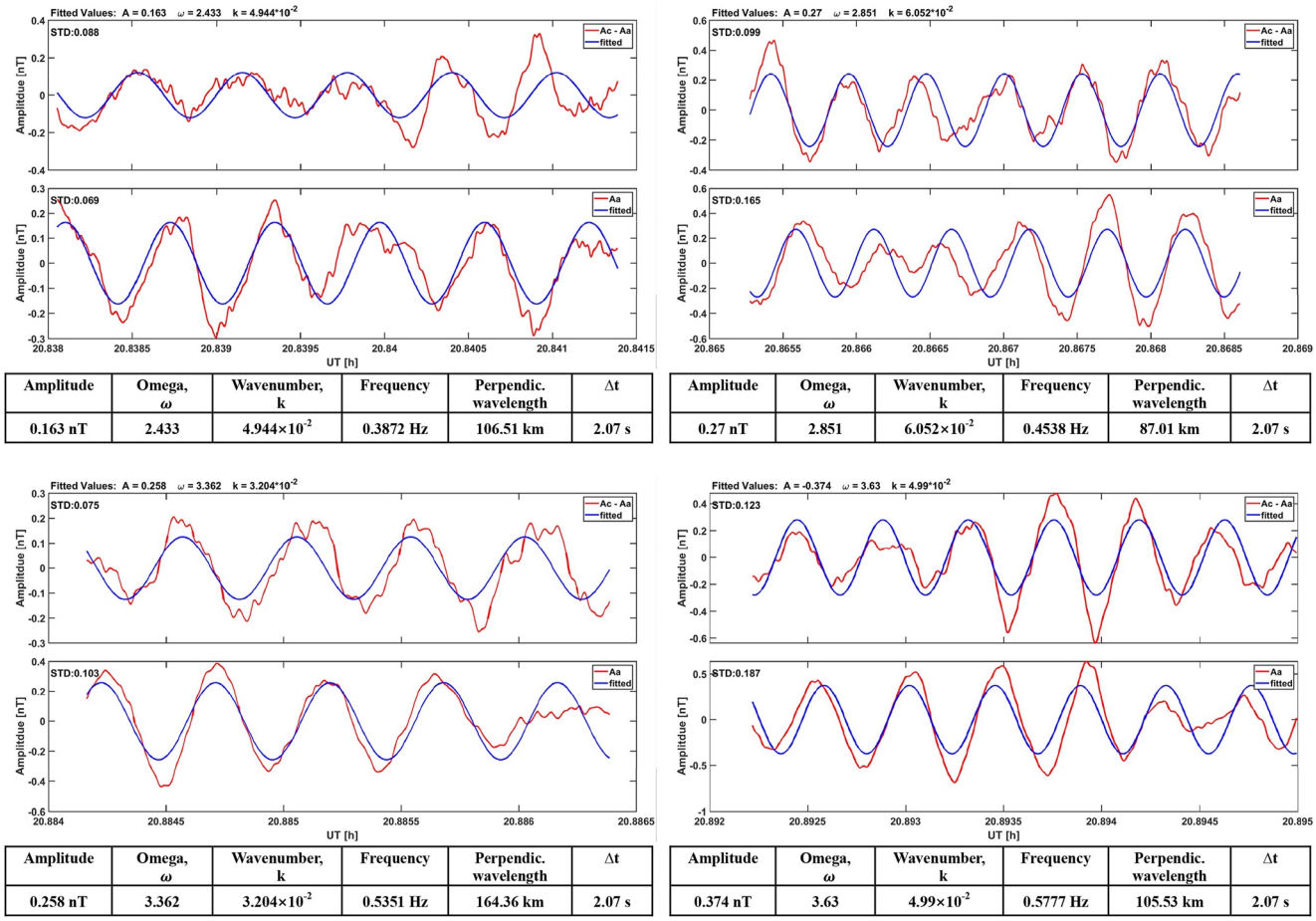

Amplitude	Omega, ω	Wavenumber, k	Frequency	Perpendic. wavelength	Δt
0.163 nT	2.433	4.944×10^{-2}	0.3872 Hz	106.51 km	2.07 s

Amplitude	Omega, ω	Wavenumber, k	Frequency	Perpendic. wavelength	Δt
0.27 nT	2.851	6.052×10^{-2}	0.4538 Hz	87.01 km	2.07 s

Amplitude	Omega, ω	Wavenumber, k	Frequency	Perpendic. wavelength	Δt
0.258 nT	3.362	3.204×10^{-2}	0.5351 Hz	164.36 km	2.07 s

Amplitude	Omega, ω	Wavenumber, k	Frequency	Perpendic. wavelength	Δt
0.374 nT	3.63	4.99×10^{-2}	0.5777 Hz	105.53 km	2.07 s

Figure 9. The same as Figure 7, but for the wave packets around 20:50:20, 20:52, 20:53, 20:53:30 UT. The derived main wave parameters are listed below the frames.

convincing EMIC event is presented by Kim et al. (2010) where the wave signal has been observed simultaneously by CHAMP and on ground at similar frequencies. Such a common detection both in the ionosphere and on ground infers that EMICs must have long wavelengths. Otherwise, the atmospheric screening would prevent a detection on ground. A plane wave in the ionosphere propagating as evanescent wave to the ground can be described as

$$\frac{b_G}{b_I} = \frac{1}{2}\frac{\Sigma_H}{\Sigma_P}\left(e^{-kh} + e^{-k(h+2d)}\right) \tag{14}$$

where b_G and b_I are the wave amplitudes on ground and in the ionosphere, Σ_H and Σ_P are the Hall and Pedersen conductances, respectively, k is wavenumber, h is height of ionosphere, and d the apparent depth of a conductosphere. When inserting typical values, for example, 2 for the conductance ratio, 110 km for h and a contribution of 30% by the induction effect to the ground signal, we can estimate the wavelength that is needed to observe on ground some signal. It requires a wavelength of order 700 km to retain on ground at least half the ionospheric amplitude.

The above quoted papers on EMIC statistics from LEO satellites did not list the Pc1 events they interpreted in terms of EMIC waves, but in all cases at least one example is shown. We have taken a closer look at five such wave cases for evaluating their characteristics. Figure 10 shows the example from Wang, He, and Lühr (2022). In the spectrogram, at the top, a clear wave feature appears near −50° MLat. It shows a center frequency at around 2.7 Hz and sidebands about 0.3 Hz above and below. This is a typical spectrum of two waves (2.4 and 3 Hz) that are interfering. In the bottom panel of Figure 10 the observed wave beating signature can clearly be seen. Another obvious feature is that the recordings of Swarm A and C are almost perfectly in phase. For determining the actual phase shift, a cross-correlation between the two signals was performed over batches of 128 points (2.56 s). A generally good correlation with a coefficient around 0.9 is achieve. Determined time lags (T-lag) are rather small varying between 0 and 60 ms.

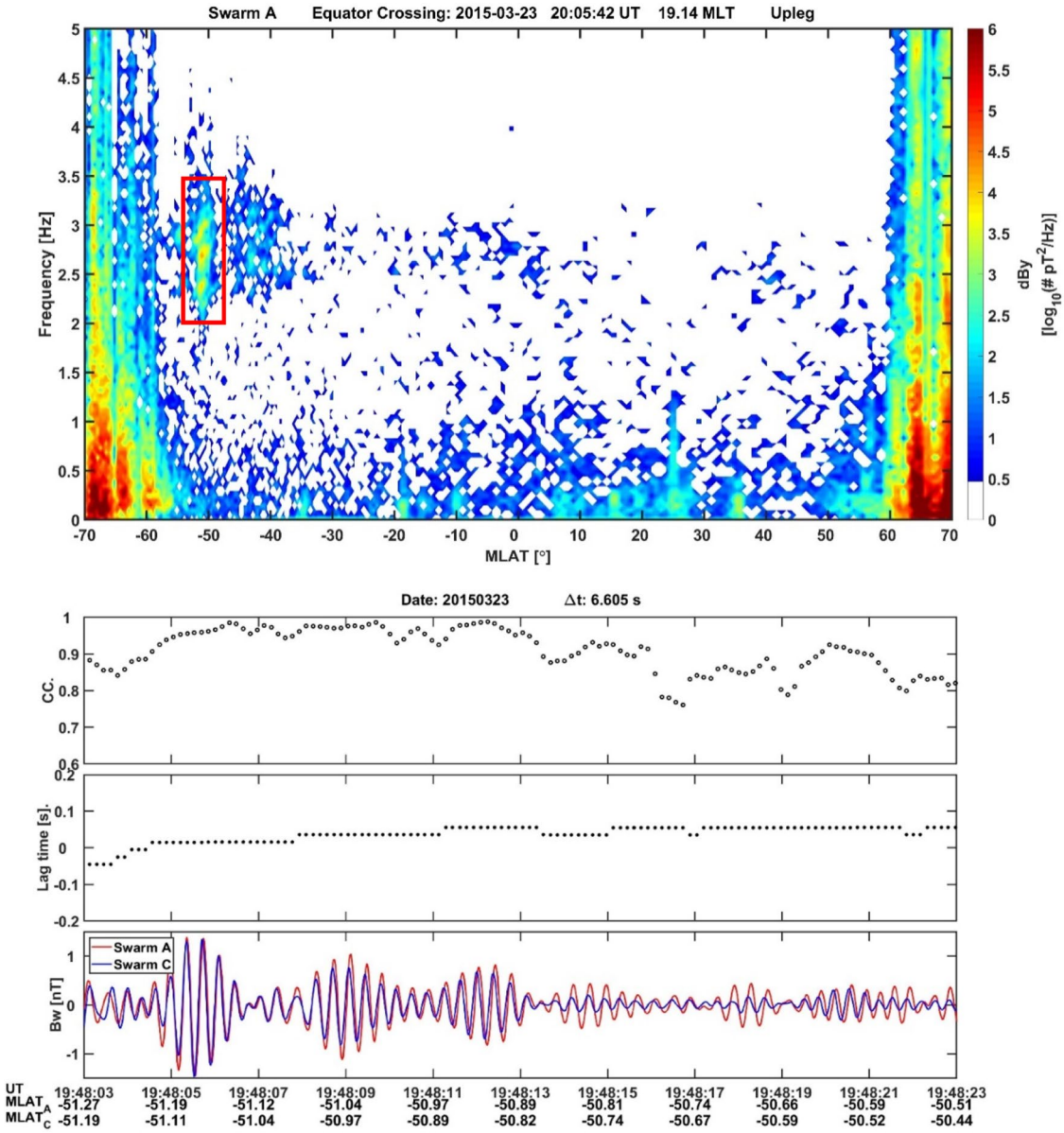

Figure 10. Dual-spacecraft investigation of an EMIC event from 23 March 2015, a published example by Wang, He, and Lühr (2022). The recordings at Swarm A and C are highly coherent, as indicated by the large cross-correlation coefficient (top panel). The middle panel displays the small shifted time by only a few ms.

All this infers really large wavelengths and consequently small wave numbers, k. For such cases the wave equations can be simplified and the term $v\,k$ ignored in the sums of Equations 3 and 4. We therefore can make use of Equations 10 and 11 for the further evaluation.

When inserting the observed quantities, such as a mean T-lag = 30 ms, the wave period, P = 370 ms, and time separation Δt = 6.6 s into Equation 13 we obtain $k = 6.86 \times 10^{-3}$ [rad/km]. From this the along-track wavelength can be computed ($\lambda = \frac{2\pi}{k}$). This results in an apparent wavelength of λ = 916 km. When considering the orientation of the wavevector (see Table 1) we get λ_{perp} = 707 km. With such a wavelength the EMIC waves should be well detectable on ground. It is interesting to note that T-lag is negative at the beginning of the presented interval in Figure 10. The shift goes through zero where the amplitude and also the wavelength are largest. The more positive the T-lag values become the smaller get the wave amplitude and also the wavelength. This suggests a relation between amplitude and wavelength with largest values at the wave center, and gradually decreasing amplitude and wavelength at latitudes away from the center.

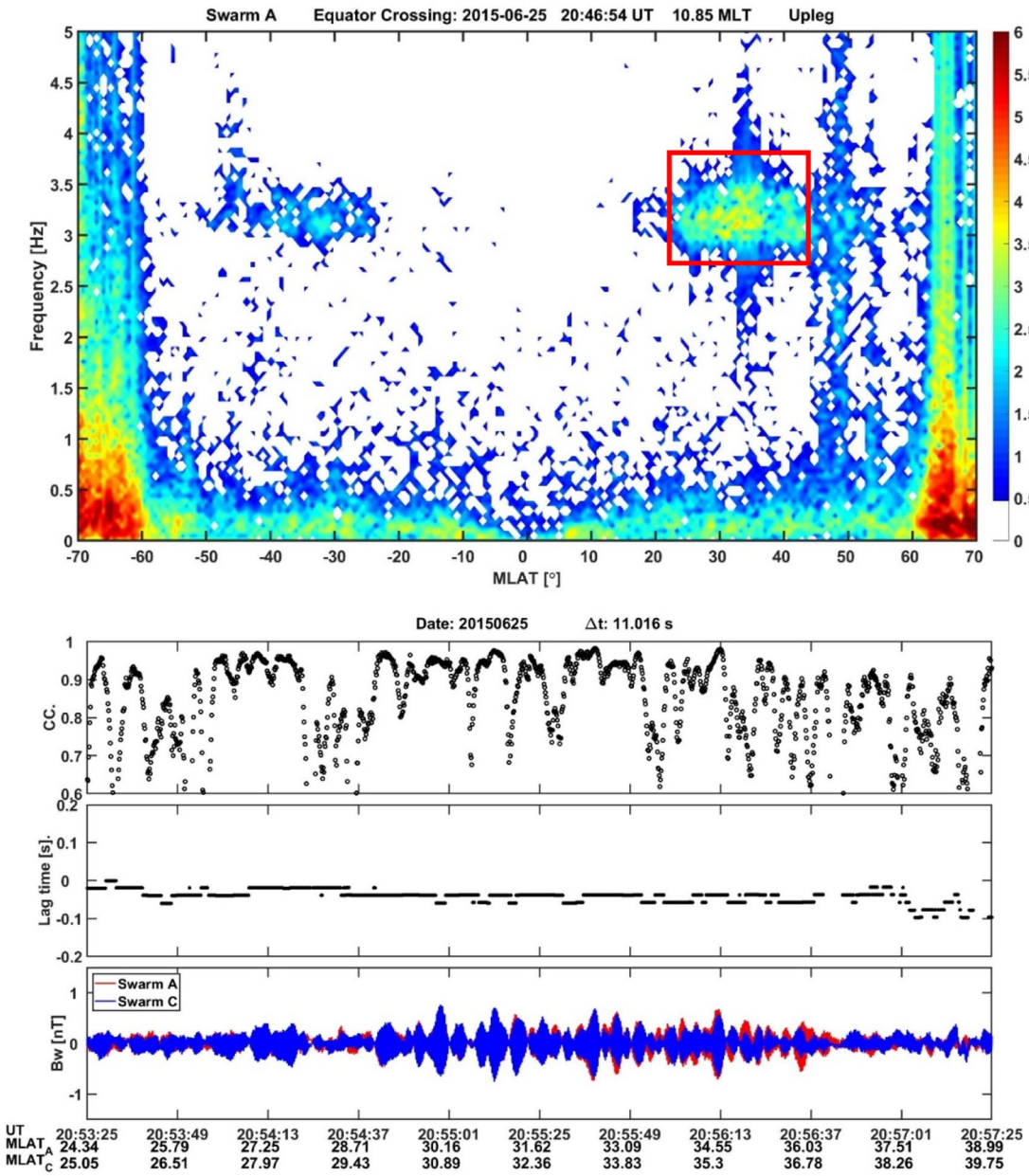

Figure 11. Same format as Figure 10, but for an EMIC example from 25 June 2015, as published by Kim et al. (2020).

A rather prominent and rather extended example of EMIC waves was presented by Kim et al. (2020). As can be seen in Figure 11, oscillations with mean frequency around 3.2 Hz reach from 25° to 40° MLat. By applying the same procedure as above, very good correlations with coefficients, mostly above 0.9, are recorded by Swarm A and C at small delays, T-lag = −20–−60 ms. When taking T-lag = −30 ms, Δt = 11 s, as derived from Figure 11, and a mean period, P = 0.31 s, we obtain a rather small $k = -4.91 \times 10^{-3}$ [rad/km]. This results again in a large apparent wavelength, λ = 1,280 km and in λ_{perp} = 980 km. Also this event satisfies well the expectations for an EMIC wave, both frequency beating and large wavelength. Here we obtained a negative k-value. This means the wave is propagating into the opposite direction compared to the previous EMIC event that gave a positive k-value. In the following section the propagation properties of the EMIC events will be discussed in more details.

We investigated further published EMIC events such as the one on 29 March 2015 from Wang, Sun, et al. (2022). From the spectrogram in Figure 12 wave activity around 1 Hz can be seen in the northern and southern hemispheres. A closer inspection by correlation analysis reveals a good match of the Swarm A and C recordings in

the northern hemisphere. Correlation coefficients are above 0.9 over large parts (whenever signals are well above noise background). Also, the phase shift within those parts is small with T-lag = 0–−60 ms.

Conversely, in the southern hemisphere the recordings of the two spacecraft do not match so well. Here a correlation coefficient of 0.9 is rarely reached. Also, the derived phase shifts, T-lag = −0.2–−0.35 s are almost an order of magnitude larger. All this indicates much reduced wavelength. Following our evaluation procedure from above, we get for the northern hemisphere with the observed parameters (P = 1.1 s, T-lag = −30 ms, Δt = 5.14 s), a wavenumber, $k = -5.93 \times 10^{-3}$ [rad/km], apparent wavelength, λ = 1,060 km, and λ_{perp} = 665 km; conversely, for the southern hemisphere (P = 1 s, T-lag = −0.25 s, Δt = 5.14 s) we obtain k = −0.041 and λ = 154 km. This indicates that the northern hemisphere event satisfies well the expectation on EMIC waves, but not the southern hemisphere case. Either another medium-scale wavelength event was traversed or the satellites passed quite far from the EMIC wave center, where the signal and wavelength is already much decayed.

Further, a Pc1 event from 25 June 2015, see Figure 13, also quoted by Wang et al. (2019) as an example for EMIC waves, shows hardly any appreciable correlation between the recordings of Swarm A and C. Neither in the northern nor in the southern hemisphere values of 0.9 are reached. Also, the derived time delays are meaningless. For that reason, this Pc1 event cannot be interpreted as EMIC waves. Some other processes must have been responsible for generating these small-amplitude Pc1 oscillations. Quite similarly, the two wave examples on 24 March 2015, presented by Wang et al. (2021), (not shown) exhibiting both poor cross-correlation coefficients and unrealistic time lags, cannot be confirmed as EMIC events by our dual-satellite approach.

4. Discussion

Here we present an initial study of wave signatures in the Swarm magnetic field recordings in the Pc1 frequency range. Details of wave properties are revealed, like the full amplitude, the degree of polarization and the orientation of the polarization ellipse with respect to magnetic east and the satellite flight direction. From the evaluation of the wave signal, simultaneously recorded by Swarm A and C, it is possible to disentangle the spatial/temporal ambiguity and derive the typical values for amplitude, frequency, and wavelength.

In the previous section it has been shown that there exists a wide range of different wave types appearing in the recordings of LEO satellites in the Pc1 frequency range. The data presented here are band-pass filtered over the range 0.2–5 Hz. Many of these signatures are caused by quasi-steady small-scale spatial features, others are slowly oscillating waves with medium wavelengths (some hundred km), and finally, the long-wavelength pulsation (order of one thousand km), which are commonly associated with EMIC waves. From single-satellite observations it is not possible to distinguish between temporal and spatial variation of the signals. For resolving this ambiguity, we employed simultaneous recordings from two closely spaced spacecraft. For this purpose, the Swarm constellation mission is very useful. In particular, the months around the counter-rotation phase with varying separations between Swarm A and C offer favorable conditions.

The general wave equation, depending both on frequency and wavelength, can in special cases be simplified. For spatial structures the slowly varying time dependence can be neglected when determining the wavelength. Conversely, for oscillations with very large wavelengths the resulting small wavenumber can be neglected in comparison to the frequency. In the latter cases, the small phase difference between recordings of the two Swarm satellites enables to determine the wavelength. For intermediate wave types, where the cycle frequency and the wavenumber are of comparable size, the full wave equation has to be solved by fitting it to the time series from the two spacecraft. Such a full-scale evaluation of the wave features in the Pc1 range is performed here for the first time.

Rather frequently, quasi-stationary spatial structures are encountered, as shown in Figures 2–5. They commonly exhibit periods of 1 s or longer in the satellite frame. For some of them we found wavelength as short as 5 km transverse to the ambient magnetic field.

Such structures are most probably caused by slowly varying field-aligned current structures. We like to interpret them in the same way, as Iyemori et al. (2015) did for their current structures in the wavelength range 70–210 km. Based on our higher resolution data set we could extend the range to significantly shorter scales. Still, we think similar generation processes are responsible. Iyemori et al. (2015) suggested that the ionospheric dynamo is driven by neutral atmospheric waves such as the acoustic gravity waves or internal gravity waves caused by lower atmospheric disturbances. These authors report on driving periods in the range of 200–300 s for their current

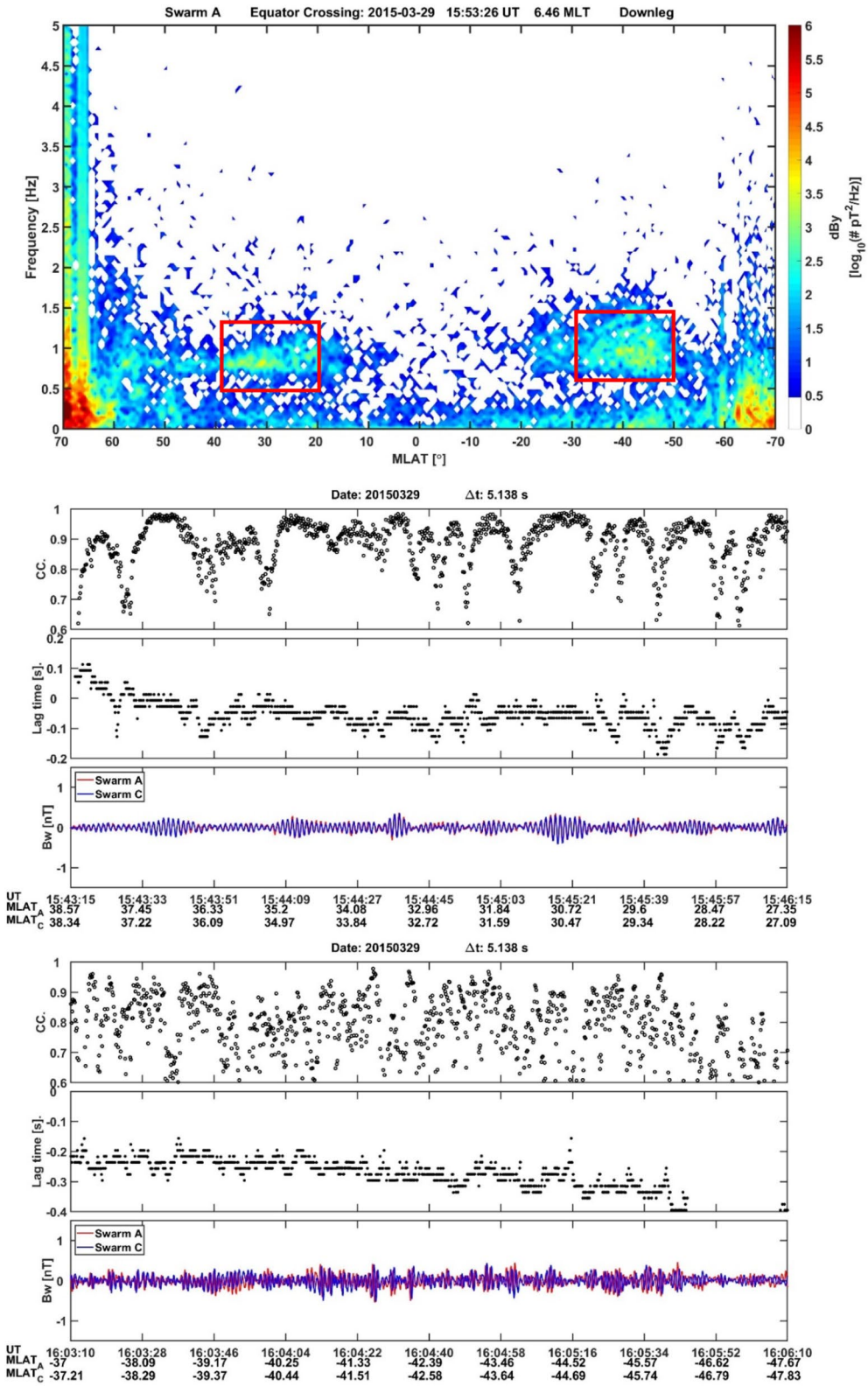

Figure 12. Same format as Figure 10, but for an EMIC example from 29 March 2015, as published by Wang, Sun, et al. (2022).

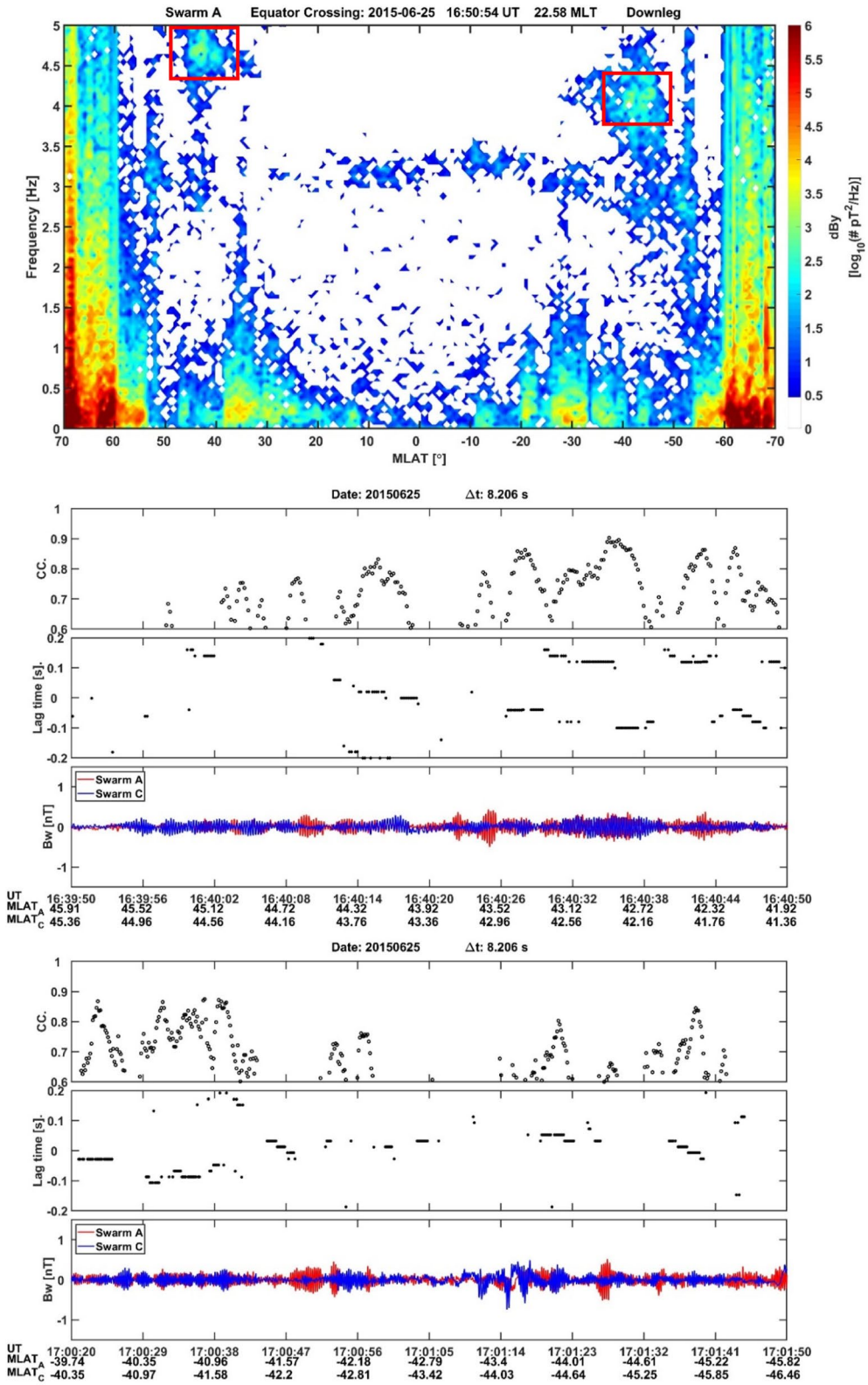

Figure 13. Same format as Figure 10, but for a wave event from 25 June 2015, as published by Wang et al. (2019). This case cannot be confirmed as EMIC waves because of poor correlation between Swarm A and C.

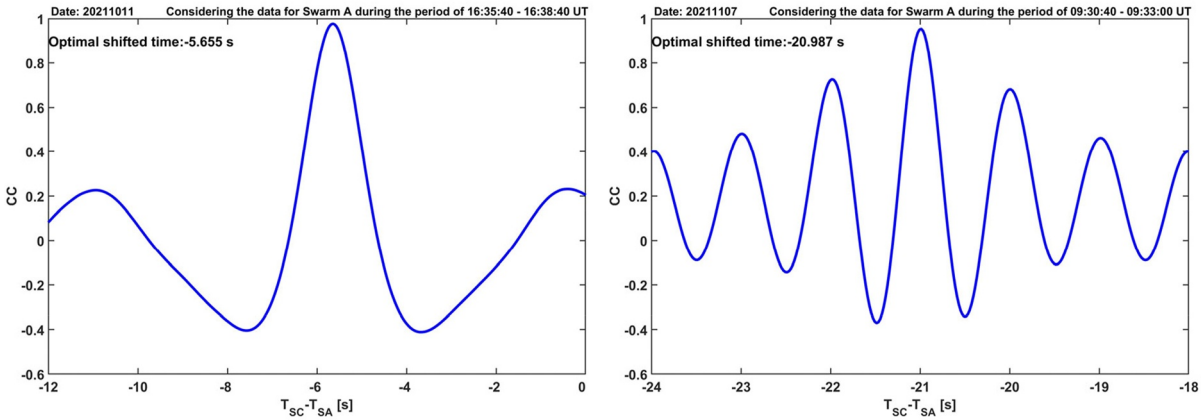

Figure 14. Variation of cross-correlation coefficient, CC, with the lag time. Presented are results from events shown in Figures 3 and 5. Sharp CC peaks appear at optimal shift between Swarm A and C signals. Derived optimal lag times have uncertainties of only ±10 ms.

structures, which cover the vertical acoustic resonance periods. Neutral atmospheric waves, generated by the lower atmospheric disturbances, are suggested as the source of the small-scale FACs.

From our two-point measurements shown in Figures 2–5, it may be possible to derive estimates of the oscillation periods for the quasi-static events. These are based on the small but significant differences between the optimal time shifts from cross-correlation and the Δt at equator crossing. As can be seen in Figure 14 for the correlation results of events from Figures 3 and 5, sharp peaks of the correlation coefficient appear at proper lag time. A detailed investigation revealed the optimal time shifts come with an uncertainty of only ±10 ms.

So far, we have neglected the frequency term for this type of wave recordings in the equation. According to Equation 4, it actually should read for Swarm C

$$\mathrm{Sw}C = A\,\cos[\omega t + v\,k(t + \Delta t)] \tag{15}$$

At optimal time shift, t_{lag}, the signal from Swarm A and C match. For that we use for Swarm C a somewhat modified time, $t' = t - t_{\mathrm{lag}}$. Then we get

$$\mathrm{Sw}C = A\,\cos\left[\omega\left(t - t_{\mathrm{lag}}\right) + v\,k(t + \delta t)\right] \tag{16}$$

where $\delta t = \Delta t - t_{\mathrm{lag}}$ is the small difference between the equator crossings and the time shift. After reordering of Equation 16 we arrive at the equation

$$\mathrm{Sw}C = A\,\cos[(\omega + v\,k)t - \omega t_{\mathrm{lag}} + v\,k\,\delta t] \tag{17}$$

For achieving a match between the Swarm A and C measurements, the last two terms in the argument have to cancel. This condition can be used to solve for ω.

$$\omega = {}^{v\,k\,\delta t}/_{t_{\mathrm{lag}}} \tag{18}$$

All the quantities on the right side can be derived from the observations. For example, vk results from the apparent frequency of the recorded wave signal. It goes beyond the scope of this study to present all the details of the derived ω-values. For all the presented quasi-stationary events we obtain real oscillation periods in the range of 100–200 s. Just the case from Figure 2 makes an exception. There we obtain about 50 s. This may be due to the very short spacecraft separation of only 2 s making the analysis most uncertain.

In this context we like to present also an event from the early mission phase, when all three spacecraft were flying in a string-of-pearls configuration. Figure 15 shows another quasi-static wave event. The signals at the three spacecraft can be matched reasonably well by considering the time differences between the satellites. For the cross-correlation we focused on the more harmonic part of the time series, for example, 17:18:00–17:18:40 UT for Swarm A. The later larger scale features exhibit different properties. As expected, the achieved correlation coefficients decrease with increasing temporal separation. Still, best matches are achieved at delay times very

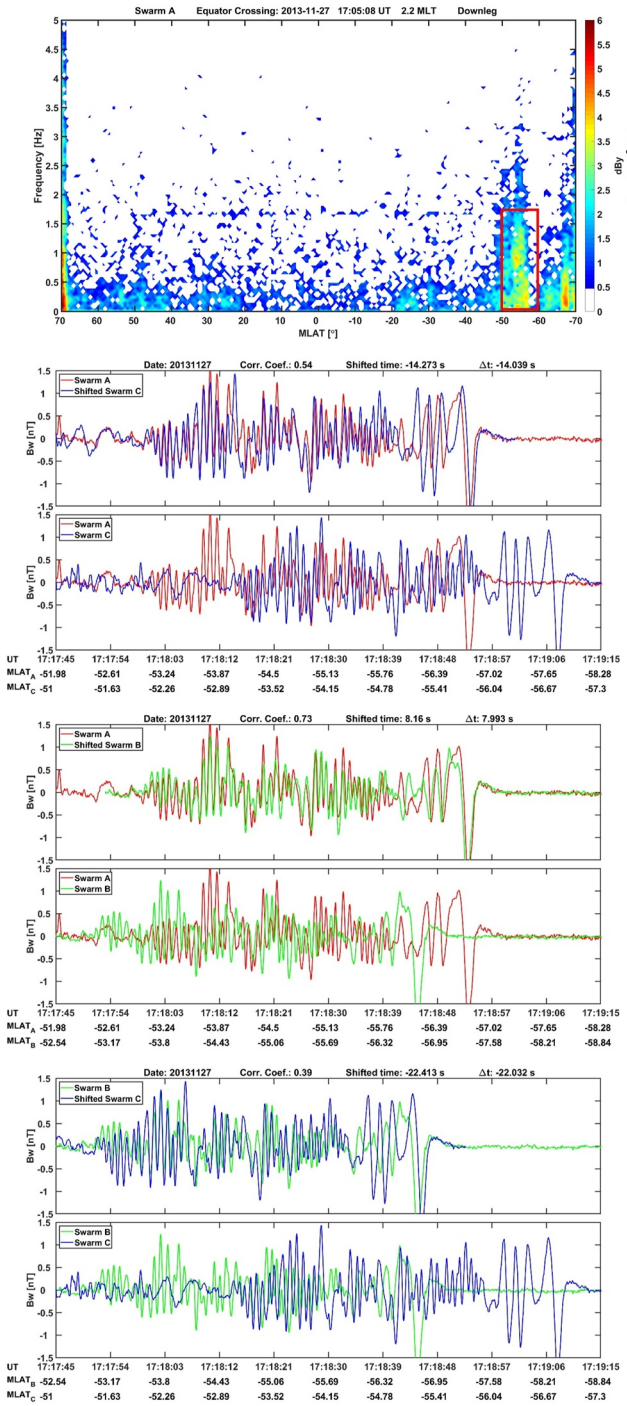

Figure 15. Example of wave signal from the early Swarm mission time when the three spacecraft followed each other as pearls on a string. The reasonable correlation between the recordings, when considering the inter-spacecraft time shifts, suggests also here a quasi-static current structure in space, similar to the cases of Figures 2–5.

close to the time differences at the equator. Here we follow the approach of Iyemori et al. (2015). When comparing the derived correlation coefficient with the related time difference we find from the three results an almost linear dependence. This is what Iyemori et al. (2015) expect from the correlation of two sinusoidal waves that slowly shift in phase. The correlation becomes zero at 90° phase shift and −1 at 180°. When we extrapolate the relation between correlation coefficient and time shift from our considered three cases linearly to an expected CC = 0, we reach at a time difference of about 40 s. Following the above argumentation, we obtain a wave period of 160 s. Also by this approach, we reach at periods within the above mentioned range. Our obtained periods are about half the value of the periods that Iyemori et al. (2015) reported for the vertical atmospheric resonance. More detailed studies of these small-scale FAC structures, possibly related to gravity waves, would be needed to resolve their spatial distribution, typical oscillation frequency, and their dependences on environmental conditions.

For the interpretation of the medium-scale waves we prefer a relation to the ionospheric Alfvén resonator. They represent standing waves between the ionosphere and an Alfvén wave velocity minimum in the lower magnetosphere (e.g., Pilipenko et al., 2002). Any external driver meeting the resonance frequency can cause the Alfvén waves to bounce between the two mirror points. A commonly high wave quality factor ensures a slow wave decay. With the satellites passing quickly through the resonance structure, we do not see the temporal evolution but rather sample the spatial width of the resonator. The traversing of individual wave packets in Figures 6 and 8 takes about 10 s, which corresponds to a distance of 75 km. From packet to packet the wave character changes, inferring that the resonance conditions are only stable over a limited latitude range, of order 1° MLat. Our wave analysis of the two presented examples reveals periods in the range of 5 to 1 s getting smaller toward lower latitudes but the transverse wavelength remains around 100 km, which is comparable with the latitudinal extend of the wave packets. Also, this type of waves is worth being studied in more details, and the Swarm dual-spacecraft observations can benefit very much such investigations.

Finally, we have checked the properties of Pc1 events that have been interpreted in earlier publications as EMIC waves. Due to their important role in modifying the energetic electron content in the radiation belt, studying EMIC waves is of great interest. One typical property of EMIC waves is their large wavelength. This makes it possible to observe them also on ground. When traversed by Swarm the two closely spaced spacecraft should practically record the same signal. From the 8 cases checked 3 clearly satisfied the expectation of large wavelengths of order 1,000 km. One event was marginal; probably Swarm passed too far from the wave center, and 4 had to be disqualified by our dual-spacecraft analysis. Already this small statistic shows the need for dedicated EMIC studies making use of multi-spacecraft wave analysis.

Along this line we present in Figure 16 another Pc1 event. In particular, the recordings of Swarm C can easily be confused with EMIC waves. As can be seen in the spectrum and the timeline plots, prominent oscillations with frequencies around 3.6 Hz are observed, and there is also the typical amplitude modulation. However, the two spacecraft record very different time series and amplitudes. Here Swarm A and C, separated in longitude by about 100 km, traverse obviously totally different wave packets. This arbitrarily picked cases and the ones shown above demonstrate the need for dual-satellite verification of EMIC events when derived from Pc1 satellite surveys.

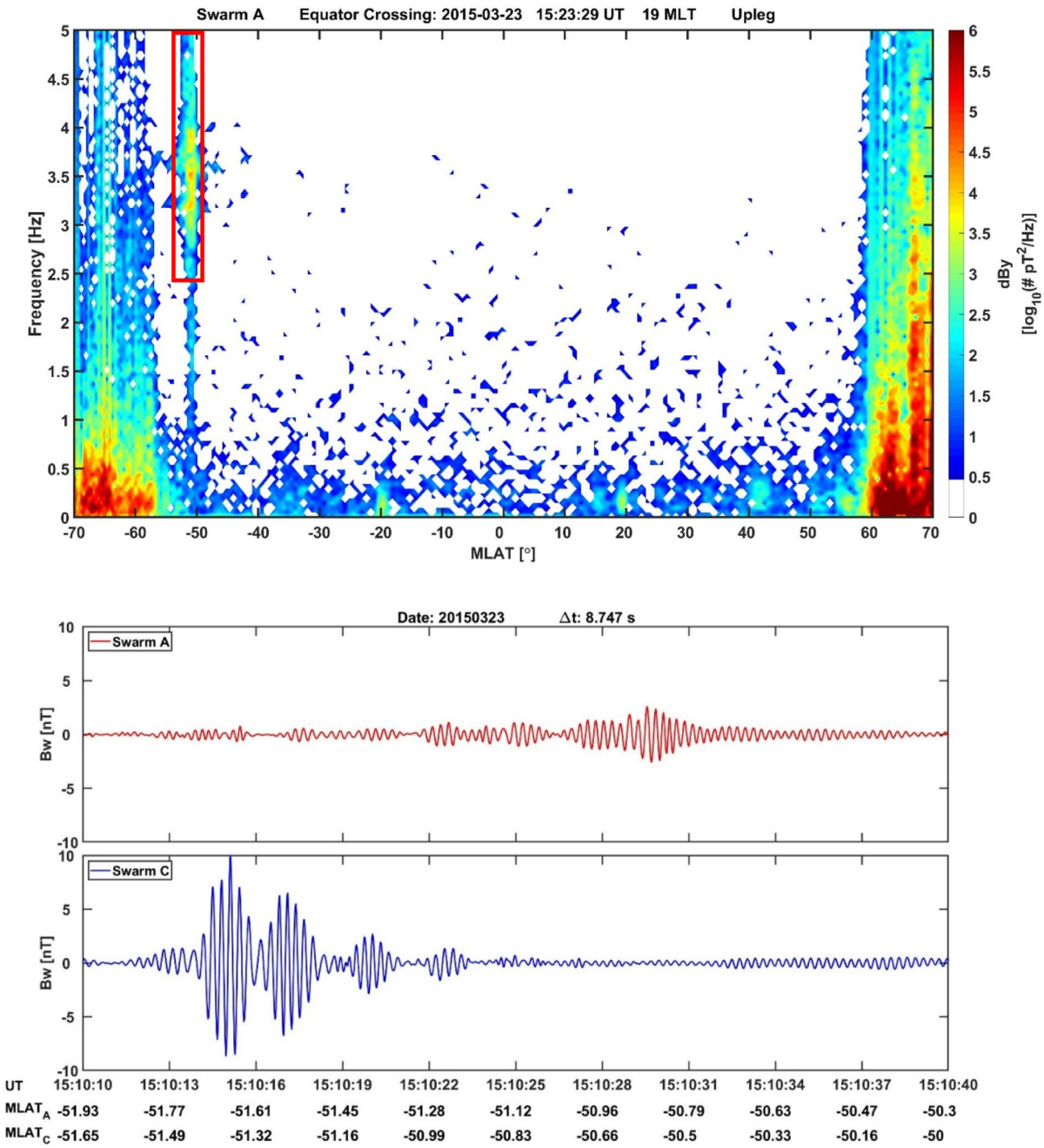

Figure 16. Example showing for Swarm C an EMIC-type wave signature, but a very different amplitude profile is observed by Swarm A. This obvious difference suggests wavelengths shorter than the spacecraft separation (<100 km), not typical for EMICs.

Another interesting result is that we can make inferences on the propagation direction of the wave from our dual-spacecraft analysis. In all the considered EMIC events Swarm C is flying ahead of Swarm A. A positive time lag gives a positive *k* value, and it means, Swarm C sees the wave crest first. From this condition follows, the wave propagates in the direction opposite to the spacecraft velocity. When turning to the event of Figure 10 we obtain for most of the time positive *T*-lag values. Since the satellites are on an upleg arc and in the southern hemisphere, the wave travels poleward. Conversely, in the case of 25 June 2015 (Figure 11) a negative *k* value implies a wave propagation in along-track direction. Here the satellites are on upleg in the northern hemisphere; thus, also that means a poleward propagation. These few examples demonstrate the amount of additional information that can be deduced from EMIC waves when studied by the Swarm A/C spacecraft pair.

5. Summary and Conclusion

This study focuses on the characterization of magnetic wave signatures in the Pc1 (0.2–5 Hz) frequency range in satellite recordings. By analyzing simultaneous B-field recording of the Swarm A and C spacecraft it is possible to resolve the spatial/temporal ambiguity of wave signatures. The apparent frequency of a wave in satellite recordings reflect just the sum, $(\omega + vk)$. Closely spaced dual-satellite observations can be used to determine the relevant wave quantities. Particularly suitable for our approach are the data from the Swarm Counter Rotating Orbit Phase in 2021. During those 6 months the along-track separation between Swarm A and C was deliberately varied between 2 and 40 s. This allowed detailed investigations of structures with different scale-lengths.

Surprisingly frequent, quasi-static current structures with rather small wavelengths of some 10 km were detected. For these variations we like to follow the interpretation of Iyemori et al. (2015) who claimed atmospheric gravity waves as the driving mechanism for such FAC structures. Here we provide an extension of the reported phenomena to smallest wavelengths down to about 6 km. Our reported periods in the range of 100–200 s are also consistent with the derived stationarity. It is worth noting that the gravity waves are obviously breaking up to small scale-lengths of only a few kilometers in the ionosphere. These observations may have implications on the proper interpretation of gravity wave characteristic.

Another class of waves was identified with medium-scale wavelength (∼100 km). Encountered proper frequencies varied around 1 Hz or slightly less. These events appear as discreate wave packets confined to certain latitude ranges. Typically, the frequency changes from packet to packet. We prefer to associate these waves with the ionospheric Alfvén resonator. If suitable excitation signal is available, the resonator will ring at a frequency within a region where resonance conditions are satisfied. It is interesting to note that the latitudinal width of the resonance region commonly agrees well with the derived wavelength of some 100 km. In more detailed studies this relation should be checked and probably interpreted.

Finally, we had a look at very long wavelengths oscillations. These pulsation in the 1–5 Hz frequency range can also be observed on ground and are commonly associated with EMIC waves. Several former studies made use of CHAMP and Swarm satellite high-resolution recordings to identify these waves. However, none of them tried to resolve the inherent spatial/temporal ambiguity. Here we checked for a number of quoted "EMIC events" in publications the actual wavelengths of those events. About half of the considered cases could be confirmed as EMIC waves, but the remaining events did not exhibit the expected similarity in the recordings of the Swarm A and C spacecraft pair. It is highly recommended that in future EMIC studies our approach for determining the main wave parameters is used for verifying the wave type before deriving statistical properties.

Data Availability Statement

The authors thank the European Space Agency for openly providing the Swarm data. The data products used in this study are Level1b MAGx_HR and MAGx_LR with version number 0602, which are available at the European Space Agency website: https://earth.esa.int/web/guest/swarm/data-access.

Acknowledgments
The work of Yun-Liang Zhou is supported by the National Nature Science Foundation of China (42174186). Open Access funding enabled and organized by Projekt DEAL.

References

Belyaev, P. P., Polyakov, S. V., Rapaport, V. O., & Trakhtengerts, V. Y. (1990). The ionospheric Alfvén resonator. *Journal of Atmospheric and Terrestrial Physics*, *52*(9), 781–788. https://doi.org/10.1016/0021-9169(90)90010-k

Denton, R. E., Anderson, B. J., Ho, G., & Hamilton, D. C. (1996). Effects of wave superposition on the polarization of electromagnetic ion cyclotron waves. *Journal of Geophysical Research*, *101*(A11), 24869–24885. https://doi.org/10.1029/96JA02251

Engebretson, M. J., Posch, J. L., Westerman, A. M., Otto, N. J., Slavin, J. A., Le, G., et al. (2008). Temporal and spatial characteristics of Pc1 waves observed by ST5. *Journal of Geophysical Research*, *113*(A7), A07206. https://doi.org/10.1029/2008JA013145

Friis-Christensen, E., Lühr, H., Knudsen, D., & Haagmans, R. (2008). Swarm—An Earth observation mission investigating geospace. *Advances in Space Research*, *41*(1), 210–216. https://doi.org/10.1016/j.asr.2006.10.008

Iyemori, T., & Hayashi, K. (1989). Pc1 micropulsations observed by Magsat in the ionospheric F region. *Journal of Geophysical Research*, *94*(A1), 93–100. https://doi.org/10.1029/JA094iA01p00093

Iyemori, T., Nakanishi, K., Aoyama, T., Yokoyama, Y., Koyama, Y., & Lühr, H. (2015). Confirmation of existence of the small-scale field-aligned currents in middle and low latitudes and an estimate of time scale of their temporal variation. *Geophysical Research Letters*, *42*(1), 22–28. https://doi.org/10.1002/2014GL062555

Kangas, J., Guglielmi, A., & Pokhotelov, O. (1998). Morphology and physics of short-period magnetic pulsations. *Space Science Reviews*, *83*(3/4), 435–512. https://doi.org/10.1023/a:1005063911643

Kim, H., Hwang, J., Park, J., Miyashita, Y., Shiokawa, K., Mann, I. R., et al. (2018). Large scale ducting of Pc1 pulsations observed by Swarm satellites and multiple ground networks. *Geophysical Research Letters*, *45*(23), 12703–12712. https://doi.org/10.1029/2018GL080693

Kim, H., Lessard, M. R., Engebretson, M. J., & Lühr, H. (2010). Ducting characteristics of Pc 1 waves at high latitudes on the ground and in space. *Journal of Geophysical Research*, *115*(A9), A09310. https://doi.org/10.1029/2010JA015323

Kim, H., Shiokawa, K., Park, J., Miyoshi, Y., Miyashita, Y., Stolle, C., et al. (2020). Ionospheric plasma density oscillation related to EMIC Pc1 waves. *Geophysical Research Letters*, *47*(15), e2020GL089000. https://doi.org/10.1029/2020GL089000

Kim, H., Shiokawa, K., Park, J., Miyoshi, Y., Stolle, C., & Buchert, S. (2021). Statistical analysis study of Pc1 wave ducting deduced from Swarm satellites. *Journal of Geophysical Research: Space Physics*, *126*(3), e2020JA029016. https://doi.org/10.1029/2020ja029016

Lysak, R. L., Waters, C. L., & Sciffer, M. D. (2013). Modeling of the ionospheric Alfvén resonator in dipolar geometry. *Journal of Geophysical Research: Space Physics*, *118*(4), 1514–1528. https://doi.org/10.1002/jgra.50090

Lysak, R. L., & Yoshikawa, A. (2006). Resonant cavities and waveguides in the ionosphere and atmosphere. In K. Takahashi, P. J. Chi, R. E. Denton, & R. L. Lysak (Eds.), *Magnetospheric ULF waves: Synthesis and new directions* (p. 289). American Geophysical Union. https://doi.org/10.1029/169GM19

Min, K., Lee, J., Keika, K., & Li, W. (2012). Global distribution of EMIC waves derived from THEMIS observations. *Journal of Geophysical Research*, *117*(A5), A05219. https://doi.org/10.1029/2012JA017515

Miyoshi, Y., Sakaguchi, K., Shiokawa, K., Evans, D., Albert, J., Connors, M., & Jordanova, V. (2008). Precipitation of radiation belt electrons by EMIC waves, observed from ground and space. *Geophysical Research Letters*, *35*(23), L23101. https://doi.org/10.1029/2008GL035727

Mursula, K., Kangas, J., & Kultima, J. (1994). Looking back at the early years of Pc1 pulsation research. *Eos*, *75*(31), 357. https://doi.org/10.1029/94eo01007

Park, J., Lühr, H., & Rauberg, J. (2013). Global characteristics of Pc1 magnetic pulsations during solar cycle 23 deduced from CHAMP data. *Annales Geophysicae*, *31*(9), 1507–1520. https://doi.org/10.5194/angeo-31-1507-2013

Pilipenko, V. A., Fedorov, E. N., & Engebretson, M. J. (2002). Alfvén resonator in the topside ionosphere beneath the auroral acceleration region. *Journal of Geophysical Research*, *107*(A9), 1257. https://doi.org/10.1029/2002JA009282

Sakaguchi, K., Shiokawa, K., Miyoshi, Y., Otsuka, Y., Ogawa, T., Asamura, K., & Connors, M. (2008). Simultaneous appearance of isolated auroral arcs and Pc1 geomagnetic pulsations at subauroral latitudes. *Journal of Geophysical Research*, *113*(A5), A05201. https://doi.org/10.1029/2007JA012888

Wang, H., He, Y., & Lühr, H. (2022). Analysis of ionospheric compressional waves and electron density oscillation during storm periods using Swarm observations. *Journal of Geophysical Research: Space Physics*, *127*(8). e2022JA030409. https://doi.org/10.1029/2022JA030409

Wang, H., He, Y. F., Lühr, H., Kistler, L., Saikin, A., Lund, E., & Ma, S. (2019). Storm time EMIC waves observed by Swarm and Van Allen Probe satellites. *Journal of Geophysical Research: Space Physics*, *124*(1), 293–312. https://doi.org/10.1029/2018JA026299

Wang, H., He, Y. F., Lühr, H., & Zhang, J. (2021). Local time and longitudinal differences in the occurrence frequency of ionospheric EMIC waves during magnetic storm periods. *Journal of Geophysical Research: Space Physics*, *126*(2), e2020JA028878. https://doi.org/10.1029/2020ja028878

Wang, H., Sun, L., Lühr, H., Liu, Y., & He, Y. (2022). Magnetic local time and latitude distribution of ionospheric large-spatial-scale EMIC wave events: Swarm observations. *Journal of Geophysical Research: Space Physics*, *127*(3), e2022JA030276. https://doi.org/10.1029/2022JA030276

Yahnin, A. G., Yahnina, T. A., Frey, H. U., Bösinger, T., & Manninen, J. (2009). Proton aurora related to intervals of pulsations of diminishing periods. *Journal of Geophysical Research*, *114*(A12), A12215. https://doi.org/10.1029/2009JA014670

Yuan, Z., Liu, K., Yu, X., Yao, F., Huang, S., Wang, D., & Ouyang, Z. (2018). Precipitation of radiation belt electrons by EMIC waves with conjugated observations of NOAA and Van Allen satellites. *Geophysical Research Letters*, *45*(12), 694–702. https://doi.org/10.1029/2018GL080481